Bioorg. Med. Chem. 95 (2023) 117490

Contents lists available at ScienceDirect

Bioorganic & Medicinal Chemistry

journal homepage: www.elsevier.com/locate/bmc

Aryl azoles based scaffolds for disrupting tumor microenvironment

Alberto Pla-López [a], Paula Martínez-Colomina [b], Laura Cañada-García [c], Laura Fuertes-Monge [d], Jose C. Orellana-Palacios [e], Alejandro Valderrama-Martínez [b], Marikena Pérez-Sosa [a], Miguel Carda [a], Eva Falomir [a,*]

[a] Departament de Química Inorgànica i Orgànica, Universitat Jaume I, E-12071 Castellón, Spain
[b] Curapath, Paterna, Spain
[c] Diversa Technologies, Santiago de Compostela, Spain
[d] Centro de Investigaciones Biológicas, CIB, CSIC, Spain
[e] Departament of Organic Chemistry, Faculty of Chemical Sciences and Technologies, University of Castilla-La-Mancha, E-13071 Ciudad Real, Spain

ARTICLE INFO

Keywords:
Triazole
Tetrazole
PD-L1
VEGFR-2
c-Myc
CD-47
IL-6
Tumor microenvironment
Antiproliferative activity
Angiogenesis

ABSTRACT

Thirty-nine aryl azoles, thirteen triazoles and twenty-seven tetrazoles, have been synthetized and biologically evaluated to determine their activity as tumor microenvironment disruptors. Antiproliferative studies have been performed on tumor cell lines HT-29, A-549 and MCF-7 and on non-tumor cell line HEK-293. It has been studied in HT-29 the expression levels of biological targets which are involved in tumor microenvironment processes, such as PD-L1, CD-47, c-Myc and VEGFR-2. In addition, antiproliferative activity was evaluated when HT-29 were co-cultured with THP-1 monocytes and the secretion levels of IL-6 were also determined in these co-cultures. The angiogenesis effect of some selected compounds on HMEC-1 was also evaluated as well as their action against vasculogenic mimicry on HEK-293. Compounds bearing an amino group in the phenyl ring and a halogen atom in the benzyl ring showed promising results as tumor microenvironment disrupting agents. The most outstanding compound decrease dramatically the population of HT-29 cells when co-cultured with THP-1 monocytes and the levels of IL-6 secreted, as well as it showed moderate effects over PD-L1, CD-47 and c-Myc.

1. Introduction

The tumor microenvironment (TME) refers to the intricate and dynamic cellular and non-cellular components present in and around a tumor mass. It plays a crucial role in the development, progression, and response of cancer[1]. The TME consists of various cell types including cancer cells, immune cells, fibroblasts, endothelial cells and other stromal cells, along with an extracellular matrix and signaling molecules. Cancer cells are the primary cells that lead to the formation of the tumor mass, which is infiltrated by various immune cells, including monocytes, T cells, B cells, natural killer (NK) cells, macrophages and dendritic cells[2]. These infiltrated immune cells play a dual role in TME as they can either trigger an antitumor immune response, attempting to eliminate the cancer cells, or they may become tolerogenic and suppress the immune response, allowing tumor growth and immune evasion. Moreover, TME is completed by the presence of endothelial cells with an angiogenic activity to provide nutrients and oxygen to the growing tumor and also by the extracellular matrix (ECM), which consists on a network of proteins, cytokines and other signaling molecules that provide structural support to the tumor and influence tumor cell behavior promoting cell growth, migration, invasion and immune responses[3].

TME has significant implications for cancer biology and therapy because an immunosuppressive environment can be originated from TME, allowing tumor cells to evade detection and destruction by the immune system. For this reason, components of TME, such as immune checkpoint molecules, angiogenic factors and pro-inflammatory cytokines, have emerged as potential targets for novel anticancer therapies. Several key components within the TME have been identified as potential targets for novel anticancer treatments, including PD-L1, CD-47, c-Myc, VEGFR-2/VEGF and IL-6[4].

PD-L1 (Programmed Death Ligand 1) is a membrane-bound protein expressed on the surface of tumor cells and immune cells within the TME. Its interaction with PD-1 (Programmed cell Death protein 1) receptor, located on T cells, leads to T cell exhaustion and immune evasion

* Corresponding author.
E-mail addresses: apla@uji.es (A. Pla-López), al413837@uji.es (P. Martínez-Colomina), al417676@uji.es (L. Cañada-García), JoseCarlos.Orellana@uclm.es (J.C. Orellana-Palacios), al407964@uji.es (A. Valderrama-Martínez), al366645@uji.es (M. Pérez-Sosa), mcarda@uji.es (M. Carda), efalomir@uji.es (E. Falomir).

https://doi.org/10.1016/j.bmc.2023.117490
Received 30 July 2023; Received in revised form 3 October 2023; Accepted 6 October 2023
Available online 14 October 2023

by the tumor. Targeting PD-L1 with immune checkpoint inhibitors, such as pembrolizumab and nivolumab, has shown remarkable success in treating various cancers, particularly those with high PD-L1 expression[5].

CD-47 is a "don't eat me" signal expressed on the surface of cancer cells. It interacts with signal regulatory protein-alpha (SIRPα) on macrophages, inhibiting phagocytosis and enabling tumor cells to evade immune surveillance[6]. Therapeutic agents that block CD-47-SIRPα interaction have demonstrated promising preclinical results enhancing macrophage-mediated tumor cell clearance and promoting antitumor immunity. Recently, it has been demonstrated that CD-47 might play vital roles in affecting immune infiltration in ovarian cancer microenvironment and it can be used as a potential target in reversing immune escape[7].

c-Myc, an oncogenic transcription factor frequently overexpressed in various cancers, regulates cell growth, metabolism, and immune response within the TME. Targeting c-Myc holds potential as a strategy to disrupt cancer-promoting signaling pathways and sensitizing tumor cells to immune-based therapies[8].

VEGF ligand and his associated receptor VEGFR-2 are involved in angiogenesis, a critical process for tumor growth and metastasis. Therapeutic approaches targeting angiogenesis include anti-angiogenic drugs and strategies focused to normalize tumor blood vessels. By inhibiting aberrant blood vessel formation, these treatments improve drug delivery to tumor site and enhance the efficacy of other anticancer agents[9]. Bevacizumab is a humanized anti-VEGF monoclonal antibody used in clinical therapies and its administration, together with other anticancer therapies, has shown synergistic effects in preclinical and clinical settings. VEGF is considered a major mediator in the induction of tumor microvasculature and it is associated with the progression, recurrency and metastasis of some types of cancer, such as non-small cell lung cancer. Targeting VEGF using monoclonal antibodies, or small molecule inhibitors, can inhibit tumor blood vessel formation leading to reduced tumor growth and increased sensitivity to other therapies[10].

VEGF is not only an important angiogenic factor but also an immunomodulator of TME. VEGFs can suppress antigen presentation, stimulate activity of regulatory T (Treg) cells, and tumor-associated macrophages, which in turn promote an immune suppressive microenvironment in NSCLC[10].

For all these reasons, targeting VEGF/VEGFR and immunotherapy are considered as novel approaches for the treatment of several types of cancer.

Finally, IL-6 is a pro-inflammatory cytokine present in TME that promotes tumor growth, survival and immune suppression[11 12]. Blocking IL-6 signaling with antibodies or small molecule inhibitors has shown promise in preclinical studies, attenuating tumor growth and enhancing the antitumor immune response[13 14].

It is clear that understanding the complex interactions within the TME is essential for developing effective cancer treatments. Targeting specific components or pathways in the TME holds promise as a strategy to enhance the effectiveness of existing therapies and develop innovative approaches to combat cancer. Therapies aimed at disrupting PD-L1, CD-47, c-Myc, VEGFR-2, VEGF and IL-6 signaling have shown significant potential in preclinical studies and clinical trials. Combining these targeted approaches with traditional treatments and immunotherapies may lead to improved outcomes for cancer patients. However, further research is necessary to optimize the efficacy and safety of these therapies and to identify multitarget molecules that disrupt TME and improve patient́s prognosis[4].

Over the last five years our research efforts have been directed towards identifying small molecules possessing both antiangiogenic and immunomodulatory properties[15 16 17]. Recently, we have extended our investigations to explore the potential impact of these novel molecules on the tumor microenvironment[18 19 20]. Among the molecules we have designed some feature a 1,2,3-triazole core intended to inhibit VEGFR-2 and PD-L1 in cancer cells (see structures A-C in Fig. 1)[16 17 18]. Notably, these compounds, with general structures A-C, have demonstrated their ability to decrease PD-L1 levels by approximately 30–40% compared to untreated cells. Additionally, certain triazole derivatives exhibited a moderate effect on c-Myc expression. Importantly, the activities observed for these compounds were comparable to VEGFR-2 inhibitors sorafenib and sunitinib[21 22], and BMS-8, a PD-L1 inhibitor[23]. Furthermore, docking studies performed by our group indicated that the triazole scaffold derivatives effectively interact with both VEGFR-2 and PD-L1 binding sites.

The present study aims to introduce structural modifications to our previously investigated molecules in order to enhance their impact on TME related proteins such as PD-L1, CD-47, c-Myc, VEGFR-2 and on the release of VEGF and pro-inflammatory cytokines such as IL-6.

Over the past decade, new scaffolds have been selected to develop novel anti-inflammatory agents with improved pharmacological profiles compared to existing ones[24]. In this regard, both triazoles and tetrazoles have emerged as promising candidates due to their wide range of

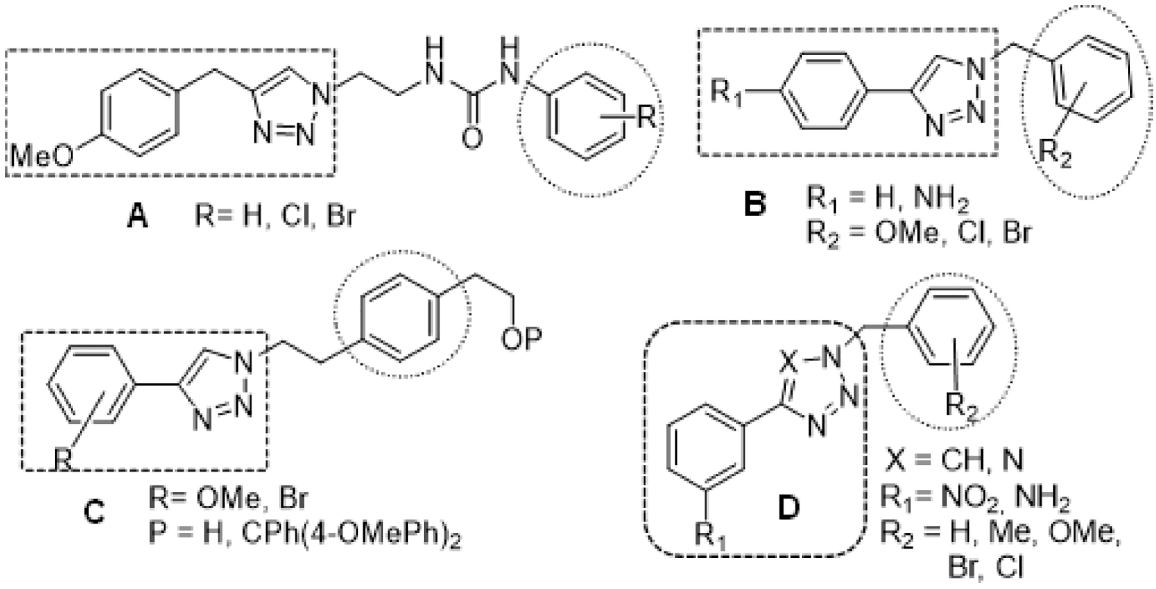

Fig. 1. General structures of molecules designed as anti-PD-L1 and VEGFR-2 agents (A-C) and proposal for new scaffolds (D) to assess their impact on various cellular activities within the tumor microenvironment (TME).

biological, pharmaceutical and clinical activities, including anticancer, antifungal, and anti-inflammatory properties[25]. Consequently, we decided to replace the *p*-aminophenyl triazole unit by a *m*-aminophenyl triazole and, also, by *m*-substituted phenyl tetrazole cores (see structure D in Fig. 1). Additionally, in the case of tetrazoles, we sought to explore the influence of the electronic nature of the phenyl substituent in these molecules by synthesizing derivatives bearing a nitro or an amino group attached to phenyl ring. The nitro group is considered to be a versatile functional group in organic and medicinal chemistry. It can undergo reduction generating more reactive species and ultimately inducing biological effects. In the last decade, the number of publications about the exploration of compounds containing nitro groups as anticancer agents, antitubercular agents, and antiparasitic agents have been increasing progressively[26 27 28] for this reason we decided to include these derivatives in our study.

Schemes 1, 2 and 3 (see below) show all the derivatives we have synthesized to assess their effects on cell proliferation, PD-L1, VEGFR-2, CD-47 and c-Myc expression in cancer cells, as well as their impact on the secretion of IL-6 in co-cultures of cancer and immune cells.

2. Results and discussion

2.1. Synthesis of triazole derivatives

Triazoles **1**–**13** were prepared by cycloaddition reaction of commercially available 3-ethynylaniline and the corresponding 1-(azidomethyl)benzene derivative in the presence of $CuSO_4{\cdot}5H_2O$ and sodium ascorbate in a 9:1 DMF/H_2O mixture (see Scheme 1). For the synthesis of the corresponding 1-(azidomethyl)benzene derivatives see Supplementary Material.

2.2. Synthesis of nitro-tetrazole derivatives

Nitro-tetrazole derivatives **14**–**26** were prepared from 5-(3-nitrophenyl)–2*H*-tetrazole which was ionized with NaH in dry CH_3CN and then reacted with benzyl halides in the presence of catalytic amounts of NaI. Some benzyl halides were achieved from the corresponding benzyl alcohol (see Supplementary Material). The rest of halides used were commercially available.

2.3. Synthesis of amino-tetrazole derivatives

Amino-tetrazoles **27**–**39** were prepared upon reduction of nitro-tetrazoles **14**–**26** mediated by zinc in glacial AcOH (see Scheme 3).

2.4. Biological evaluation

2.4.1. Study of the effect on cell proliferation

The ability of synthetized derivatives **1**–**39** to inhibit the proliferation of cancer cells was measured by MTT assay on cancer cells HT-29 (colon adenocarcinoma), A-549 (lung adenocarcinoma) and MCF-7 (breast adenocarcinoma) and on non-cancer cell line HEK-293. IC_{50} values were achieved after 48 h of treatment with the corresponding compounds. Table 1 shows the IC_{50} values for the most active derivatives. The rest of the compounds exhibited IC_{50} values higher than 100 μM.

None of the triazole derivatives exhibited antiproliferative action in monocultures of the tested cell lines and for the tetrazole ones a very moderated action was measured, with some compounds yielding IC_{50} values above 35 μM. It is worth to mention that tetrazole derivatives **23** and **36**, bearing a *p*-bromobenzylic unit, were the only ones that showed IC_{50} values below 50 μM (see Table 1).

2.4.2. Effect on the expression of PD-L1, c-Myc and VEGFR-2 on HT-29

The purpose of this study was to screen the synthetized compounds according to their effect on the presence of the immune checkpoint PD-L1 on the cell surface and, also, in the whole cells; on c-Myc, which is a crucial protein for the regulation of TME and on the angiogenic factor VEGFR-2. In the case of VEGFR-2 we also studied the presence of this protein in the cell surface and in the cell. The study was performed by treating HT-29 cells with 100 μM doses of all the synthetized compounds **1**–**39** for 48 h. Then, we determined by flow cytometry the relative expression of the mentioned targets compared to non-treated cells (control). Table 2 shows those compounds that exhibited any effect on the expression of: membrane PD-L1 (*m*PD-L1), PD-L1 in the whole cell (*t*PD-L1), c-Myc, *m*VEGFR-2 and *t*VEGFR-2. The rest of the compounds had no effect.

In general, none of the compounds showed any effect on the expression of PD-L1 in cancer cells (see column 3 in Table 2) but some compounds were capable to diminish the presence of this target on the cell surface (see column 2 in Table 2). In this sense, the most outstanding compounds are nitro-tetrazole **14**, bearing no substituent in the benzylic unit, nitro-tetrazoles **15**–**17** bearing a methyl group in the benzylic unit, and amino-tetrazoles **34** and **35** bearing in the benzylic ring a bromine in *ortho* or *meta* position, respectively. The above-mentioned compounds showed inhibition rates around 45 % related to control.

As regards c-Myc, nitro-tetrazoles **17** (*p*-Me), **19** (*m*-OMe) and **23** (*p*-Br) together with amino-tetrazoles **36** (*p*-Br), **38** (*m*-Cl) and **39** (*p*-Cl) were the most active reducing the expression of this protein to about 75

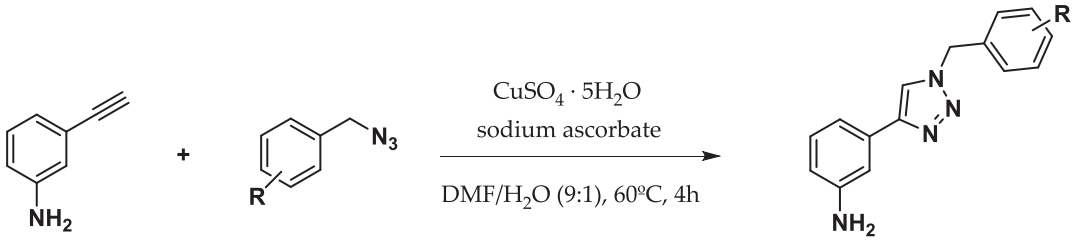

1	(20%)	R = H	**8**	(38%)	R = *o*-Br
2	(63%)	R = *o*-CH_3	**9**	(65%)	R = *m*-Br
3	(62%)	R = *m*-CH_3	**10**	(17%)	R = *p*-Br
4	(76%)	R = *p*-CH_3	**11**	(42%)	R = *o*-Cl
5	(55%)	R = *o*-OCH_3	**12**	(78%)	R = *m*-Cl
6	(59%)	R = *m*-OCH_3	**13**	(20%)	R = *p*-Cl
7	(69%)	R = *p*-OCH_3			

Scheme 1. Synthesis of functionalized triazoles **1**–**13**.

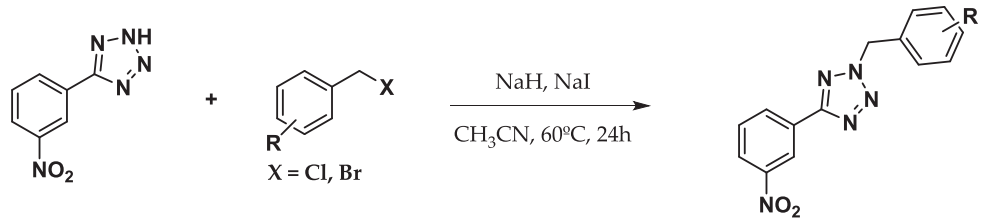

14	(65%)	R = H	**21**	(30%)	R = *o*-Br
15	(24%)	R = *o*-CH_3	**22**	(17%)	R = *m*-Br
16	(61%)	R = *m*-CH_3	**23**	(58%)	R = *p*-Br
17	(67%)	R = *p*-CH_3	**24**	(48%)	R = *o*-Cl
18	(56%)	R = *o*-OCH_3	**25**	(66%)	R = *m*-Cl
19	(24%)	R = *m*-OCH_3	**26**	(72%)	R = *p*-Cl
20	(48%)	R = *p*-OCH_3			

Scheme 2. Synthesis of functionalized nitro-tetrazoles **14**–**26**.

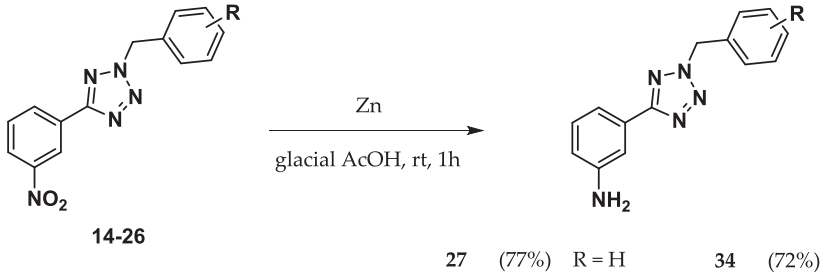

27	(77%)	R = H	**34**	(72%)	R = *o*-Br
28	(76%)	R = *o*-CH_3	**35**	(62%)	R = *m*-Br
29	(76%)	R = *m*-CH_3	**36**	(78%)	R = *p*-Br
30	(76%)	R = *p*-CH_3	**37**	(80%)	R = *o*-Cl
31	(65%)	R = *o*-OCH_3	**38**	(78%)	R = *m*-Cl
32	(53%)	R = *m*-OCH_3	**39**	(76%)	R = *p*-Cl
33	(65%)	R = *p*-OCH_3			

Scheme 3. Synthesis of functionalized amino-tetrazoles **27**–**39.**

Table 1
IC_{50} values (μM) for the most active derivatives.

Comp.	HT-29	A-549	MCF-7	HEK-293
23	>100	39 ± 1	>100	>100
24	81 ± 12	>100	>100	>100
26	>100	>100	84 ± 7	>100
36	>100	>100	44 ± 1	>100
38	81 ± 12	>100	88 ± 8	>100
39	72 ± 41	>100	>100	91 ± 22

IC_{50} values are expressed as the compound concentration that inhibits the cell growth by 50%. Data are the average (±SD) of three experiments.

% related to control. Nitro and amino-tetrazoles bearing a bromine in *para* position of the benzyl group were between the most active ones.

Finally, we found that none of the compounds had effect on the presence of VEGFR-2 on the cell surface but we found nitro-tetrazoles **18**–**20** (OMe), **22** (*m*-Br), **24** (*o*-Cl) and **26** (*p*-Cl) as the ones able to inhibit VEGFR-2 total expression more than 45 % related to control.

2.4.3. Effect of the compounds on cell viability in co-cultures of HT-29 and THP-1

We also studied the effect of all the synthetized compounds on cancer cell viability of HT-29 cells in the presence of circulating THP-1 immune cells. For this assay, HT-29 cells were treated for 48 h with the selected compounds at 100 μM in presence of interferon γ stimulated THP-1

Table 2
Relative amount of *m*PD-L1, *t*PD-L1, c-Myc, *m*VEGFR-2 and *t*VEGFR-2 compared to control (%) for the most active compounds.

Comp.	*m*PD-L1	*t*PD-L1	c-Myc	*m*VEGFR-2	*t*VEGFR-2
14	66 ± 1	>100	82 ± 12	>100	>100
15	64 ± 4	94 ± 9	91 ± 18	>100	72 ± 21
16	65 ± 2	97 ± 10	89 ± 17	>100	84 ± 47
17	63 ± 5	92 ± 9	78 ± 16	>100	65 ± 28
18	89 ± 2	92 ± 24	86 ± 6	>100	55 ± 6
19	83 ± 17	>100	75 ± 6	>100	42 ± 1
20	84 ± 2	89 ± 6	>100	88	39 ± 14
21	>100	97 ± 9	90 ± 8	>100	75 ± 6
22	>100	88 ± 12	76 ± 2	100 ± 0	60 ± 6
23	>100	93 ± 11	72 ± 4	96 ± 1	71 ± 3
24	98 ± 1	89 ± 13	86 ± 4	97 ± 2	53 ± 13
25	>100	90 ± 20	>100	97 ± 3	>100
26	93 ± 2	87 ± 8	90 ± 20	95 ± 2	45 ± 28
29	>100	81 ± 8	>100	>100	>100
31	97 ± 6	>100	97 ± 10	99 ± 12	>100
32	>100	>100	86 ± 7	76 ± 2	>100
33	>100	99 ± 16	75 ± 8	>100	75 ± 2
34	64 ± 1	>100	90 ± 16	>100	92 ± 34
35	66 ± 6	>100	83 ± 15	>100	>100
36	92 ± 21	>100	76 ± 14	>100	>100
37	95 ± 1	>100	>100	96 ± 1	92 ± 6
38	>100	97 ± 11	76 ± 6	97 ± 2	99 ± 8
39	>100	99 ± 14	80 ± 6	>100	96 ± 7

monocytes. Then, the relative number of living cells were determined by flow cytometry. Fig. 2 shows the relative number of living cancer cells when treated with the corresponding compounds compared to control.

Data presented in Fig. 2 show that, in general, all the derivatives had an immunomodulatory effect, since in monocultures their ability to reduce cancer cell viability was very low, whereas in co-cultures of cancer cells and THP-1 monocytes they reduced cancer cell viability to less than half of the control cells. It is interesting to note that monocytes from the co-cultures were not affected by this immunostimulant action of the compounds (see Figure 2S in Supporting Information for the relative number of THP-1 cells from co-cultures after the treatment with the corresponding compounds).

As far as the structure–activity relationship is concerned, it can be observed that, in general, derivatives with *meta-* and *para-* substituents on the benzyl group are the most active ones inhibiting cancer cell viability in co-cultures, the latter being the most actives.

In addition, the effect is more pronounced when the benzylic substituent bears a halogen, e.g. triazoles **9** (*m*-Br), **10** (*p*-Br), **12** (*m*-Cl) and **13** (*p*-Cl) and amino-tetrazoles **35** (*m*-Br) and **36** (*p*-Br), all showing inhibition rates higher than 90 %. Among the other derivatives, tetrazoles are, generally, more active than triazoles. The activity of nitro-tetrazoles **17** (*p*-Me) and **22** (*m*-Br) and aminotetrazoles **28** (*o*-Me), **29** (*m*-Me) and **30** (*p*-Me), **34** (*o*-Br), **35** (*m*-Br) and **39** (*p*-Cl) should not be underestimated, all of them exhibiting inhibition rates above 70 %.

Fig. 3 shows pictures of HT-29 cells co-cultured with monocytes after 48 h of treatment with a selection of compounds (**10**, **13**, **18**, **19**, **20**, **31**, **32** and **33**) at 100 μM doses. As it can be appreciated, the number of cells is lower than in the control and the morphology of cancer cells has dramatically changed. Thus, treatment provokes a shrinkage of cells and the adoption of a rounded morphology.

2.4.4. Study of the effect on the biological targets PD-L1 and CD-47 on cancer cells co-cultured with THP-1 monocytes

The aim of this study was to assess the effect of our compounds on the immune checkpoints PD-L1 and CD-47 in cancer cell membrane. Fig. 4 shows the relative amount of both proteins related to non-treated cells for all the compounds. All derivatives were tested at 100 μM.

It can be observed that, in general, our compounds had a moderated action in the inhibition of CD-47 expression on cell surface, whereas no effect was observed on PD-L1. Amino-tetrazoles were the most active with **29** (*m*-Me), **30** (*p*-Me), **33** (*p*-OMe), **34** (*o*-Br), **35** (*m*-Br) and **36** (*p*-Br) exhibiting more than 30 % CD-47 inhibition. Importantly, these last three compounds also inhibit the presence of PD-L1 on the cell surface by 70%. Again, *meta-* and *para-* derivatives are more active than *ortho-* ones and halogenated compounds are the ones with most outstanding results in both surface targets.

2.4.5. Study of the effect on the IL-6 secreted into the medium in HT-29 and THP-1 co-cultures

We selected some of the most outstanding compounds from the co-

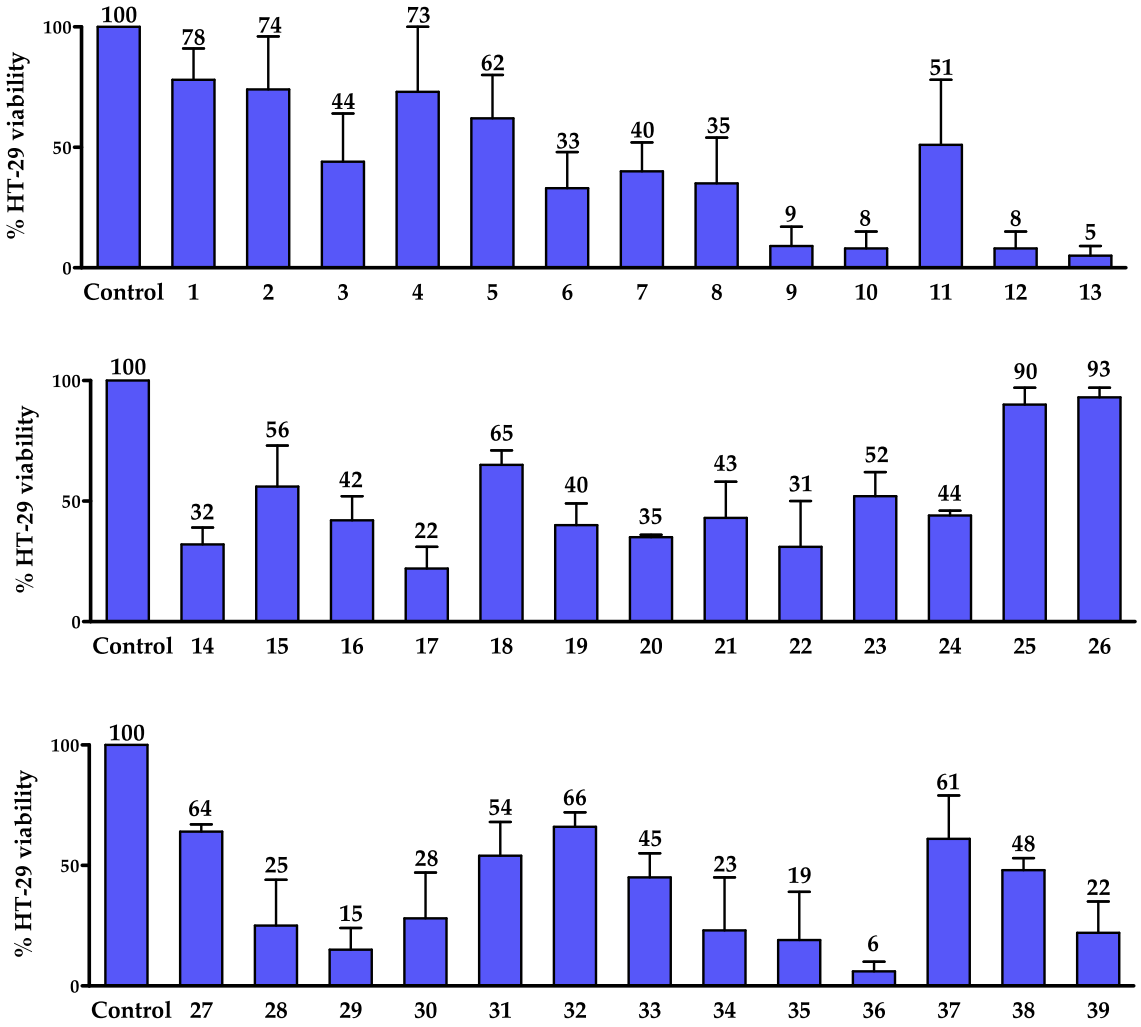

Fig. 2. Relative number of HT-29 cells when co-cultured with THP-1 (%).

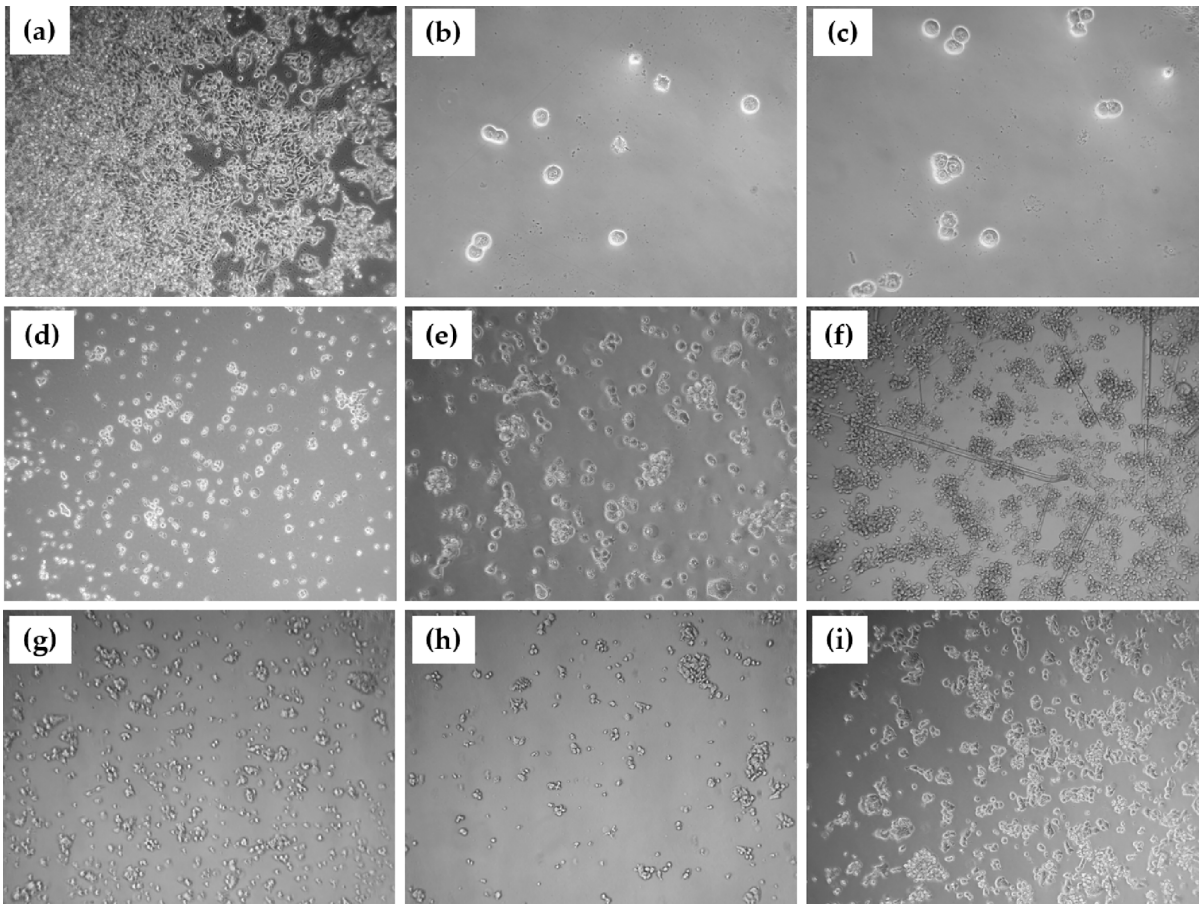

Fig. 3. Effect of selected compounds on the morphology of HT-29 cells after 48 h of treatment with 100 μM doses of: (a) DMSO, (b) **10**, (c) **13**; (d) **18**, (e) **19**, (f) **20**, (g) **31**, (h) **32**, (i) **33**.

culture studies to assess their effect on the secretion of IL-6 into the cell medium. Compounds selected were triazoles **10** (*p*-Br), **11** (*o*-Cl), **12** (*m*-Cl) and **13** (*p*-Cl) and amino-tetrazoles **36** (*p*-Br), **37** (*o*-Cl), **38** (*m*-Cl) and **39** (*p*-Cl). We measured the level of IL-6 secreted into the cell medium from monocultures of HT-29 cells and, also, from co-cultures of HT-29 and THP-1 after 48 h of treatment with the selected compounds at 100 μM doses. Measurements were carried out by ELISA assay and showed that none of the compounds had any effect on the level of IL-6 secreted into HT-29 monocultures. However, a very pronounced effect on cytokine secretion was observed when HT-29 cells were cultured in the presence of THP-1 monocytes (see Table 3).

Again, tetrazoles were more active than triazoles. Nevertheless, triazoles **11** (*o*-Cl) and **12** (*m*-Cl) showed more than 80 % inhibition of IL-6 secretion, whereas all the selected halo-tetrazoles decreased more than 95 % the level of IL-6 in the co-cultures medium.

As IL-6 is primarily a pro-tumorigenic cytokine that, when present at high levels in TME, promotes tumor cell growth and tumor cell migration, data yielded by this study demonstrate the potential of the compounds developed in this work as disrupting-TME agents.

2.4.6. *Study of the antiangiogenic effect of selected compounds*

For this study, we selected those derivatives with the best results in co-culture studies to determine their ability to block the formation of new vascular network and to disrupt the microvascular network that has already been formed. Selected compounds were triazole **10** (*p*-Br) and **13** (*p*-Cl) and haloamino-tetrazoles **34**–**39**. Firstly, we studied the antiangiogenic activity by seeding HMEC-1 cells on Matrigel® that, simultaneously, were treated at 100 μM doses of the selected compounds. At this non-cytotoxic dose, compounds yielded excellent results. Pictures were taken 24 h later to evaluate the tube formation inhibition effect. We observed that all the tested compounds were able to inhibit the formation of endothelial microtubes (see Fig. 5). The antiangiogenic effect was mild at concentrations below 75 μM.

Having established the strong anti-angiogenic potential of these compounds, we decided to go a step further to test their potential anti-TME action. In recent years, it has been described that in the development of a tumor mass, a phenomenon called vasculogenic mimicry (VM) occurs[29]. Vasculogenic mimicry is the ability of tumor cells to form vessel-like networks that provide adequate blood supply for tumor growth. Additionally, cancer stem cells and epithelial-mesenchymal transitions are also shown to be implicated in VM formation. VM is associated with tumor invasion, metastasis and poor cancer patient prognosis[30 31].

As an approximation to the potential action of the selected compounds against VM, we carried out an assay by seeding HEK-293 cells on Matrigel® and, after 24 h of incubation at 37 °C, tube-like structures were detectable, and the selected compounds were added at 100 μM doses. After 24 h, we observed for most of the cases the disruption of the tube-like structures (see Fig. 6). Again, the antivasculogenic effect was mild at concentrations below 75 μM.

3. Conclusion

As conclusion of all this study, we have developed a series of compounds with a tetrazole or triazole template that are capable of blocking cancer cells growth through their immunomodulatory, anti-inflammatory, antiangiogenic and antivasculogenic effects. The presence of a *m*-aminophenyl group and a *m*- or *p*-halobenzyl group on the

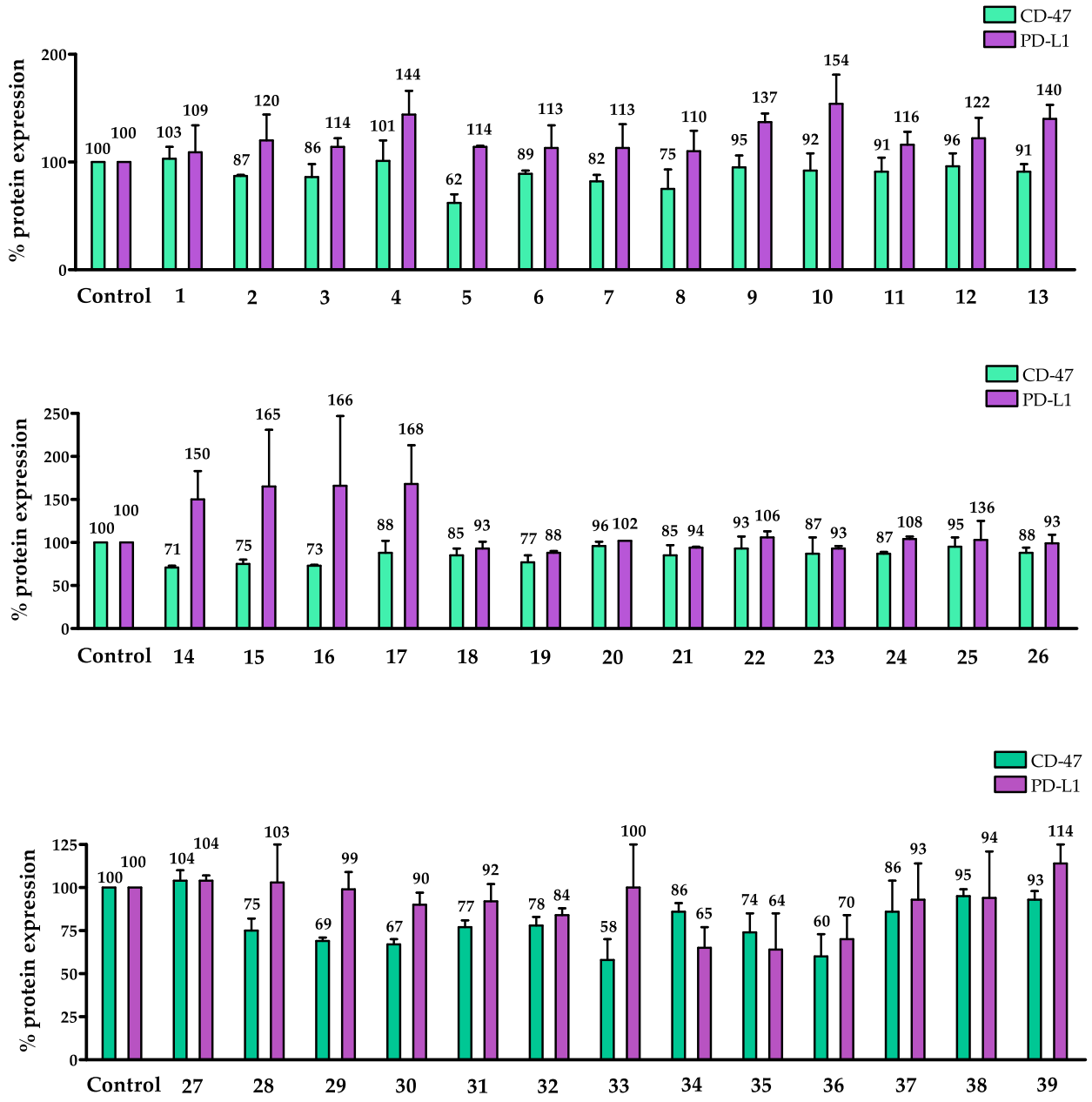

Fig. 4. Relative amount (%) of surface CD-47 and PD-L1 compared to control.

Table 3
Concentration of IL-6 in cell media from co-cultures HT-29/THP-1 and relative amount of IL-6 compared to control. Data are the average of three experiments.

Comp.	IL-6 Concentration (pg/mL)	IL-6 % relative amount
Control	192 ± 16	100
10	183 ± 19	95
11	12 ± 2	6
12	38 ± 5	20
13	189 ± 21	98
36	5 ± 1	3
37	6 ± 1	3
38	6 ± 1	3
39	11 ± 3	6

tetrazole ring enhances their action. Among all, the most outstanding of them is tetrazole **36** because, at 100 μM dose, it is not cytotoxic, but it is able to enhance immune system to reduce the presence of living cancer cells to 5%, to reduce the expression of PD-L1 and CD-47 to around 65%, to reduce c-Myc expression in cancer cells to 75 % and IL-6 levels in co-culture medium to 3% and to inhibit the formation of new microvessels and the vasculogenic effect. So, we assume this set of compounds are promising TME-disturbing agents.

4. Experimental section

4.1. Chemistry

4.1.1. General procedures

^{1}H and ^{13}C NMR spectra were measured at 25 °C. The signals of the deuterated solvent ($CDCl_3$ and DMSO-d_6) were taken as the reference. Multiplicity assignments of ^{13}C signals were made by means of the DEPT pulse sequence. Complete signal assignments in ^{1}H and ^{13}C NMR spectra were made with the aid of 2D homo- and heteronuclear pulse sequences (COSY, HSQC, HMBC). Infrared spectra were recorded using KBr plates.

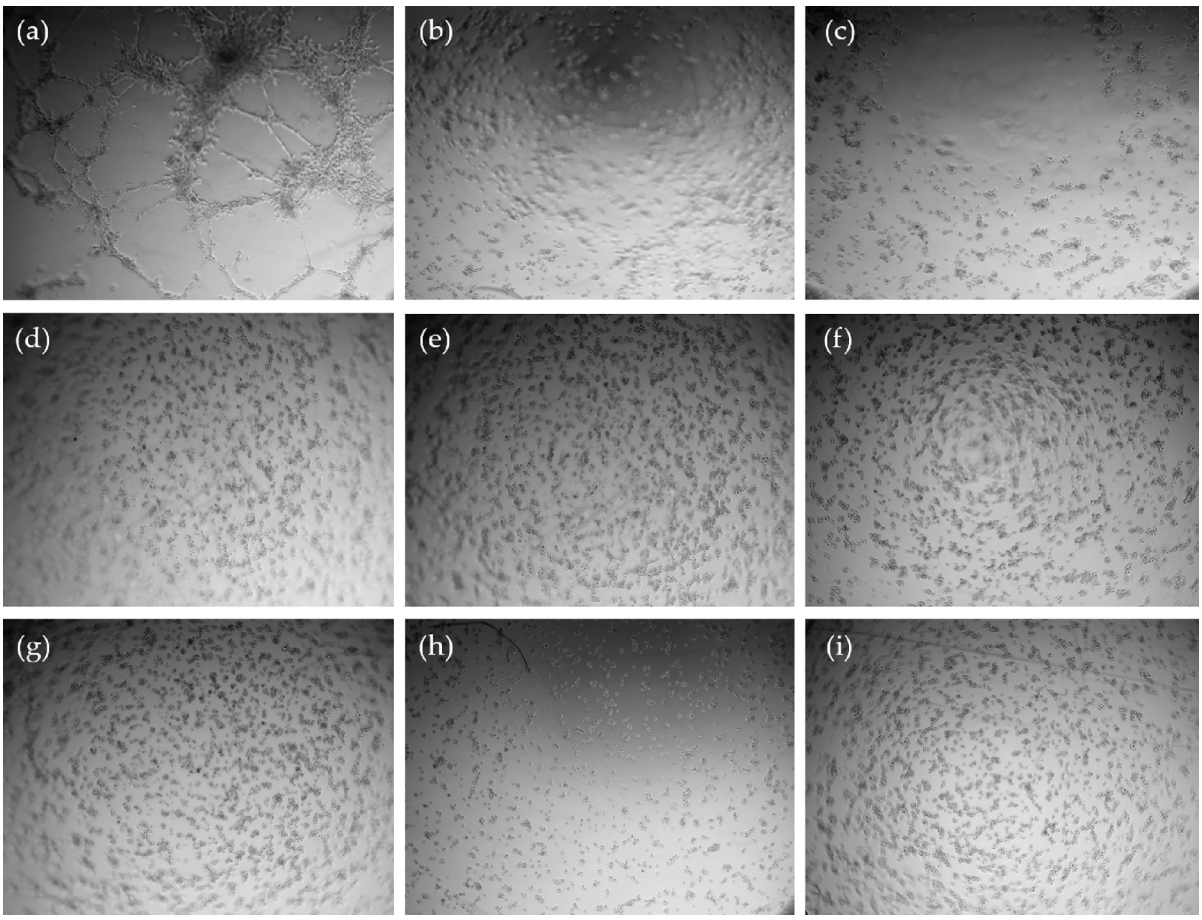

Fig. 5. Antiangiogenic effect after 24 h of (a) DMSO; (b) **10** (100 μM); (c) **13** (100 μM); (d) **34** (100 μM); (e) **35** (100 μM); (f) **36** (100 μM); (g) **37** (100 μM); (h) **38** (100 μM); (i) **39** (100 μM).

High resolution mass spectra were recorded using electrospray ionization–mass spectrometry (ESI–MS). Experiments which required an inert atmosphere were carried out under dry N_2 in oven-dried glassware. Commercially available reagents were used as received.

*4.1.2. Experimental procedure for the synthesis of compounds **1–13***

A solution of 3-ethynylaniline (2.5 mmol, 1 eq.) with the corresponding 1-(azidomethyl)benzene derivative (3 mmol, 1.2 eq.) in DMF/H_2O (9:1, 25 mL) was stirred at 60 °C for 4 h in the presence of $CuSO_4{\cdot}5H_2O$ (0.25 mmol) and sodium ascorbate (0.25 mmol). Then, the reaction mixture was poured onto ethyl acetate (20 mL) and brine (10 mL) was addded. The aqueous phase was extracted with ethyl acetate (3 × 10 mL) and the collected organic phases were washed with brine and dried over anhydrous Na_2SO_4. Filtration and removal of the solvent under vacuum afforded a residue that was purified on column chromatography using silica gel as stationary phase and a mixture of hexane: ethyl acetate (1:1) as mobile phase.

*4.1.3. Experimental procedure for the synthesis of compounds **14–26***

A NaH suspension in mineral oil (0,5 mmol, 1 eq.) was washed with pentane (3 × 1.25 mL) under inert atmosphere. After cooling at 0 °C, dry acetonitrile (3 mL) was added and the mixture was stirred for 5 min. Then, a solution of the corresponding tetrazole (0.5 mmol, 1 eq.) in the minimum quantity of acetonitrile was added. The reaction mixture was stirred at room temperature for 30 min and then the corresponding benzyl halide (0.55 mmol, 1.1 eq.) and a catalytic amount of NaI were added. The reaction mixture was allowed to react at 60 °C for 24 h. Then, it was poured onto an aqueous saturated solution of NH_4Cl (10 mL). The aqueous phase was extracted with ethyl acetate (3 × 10 mL) and the collected organic phases were washed with brine and dried over anhydrous $MgSO_4$. After solvent elimination under vacuum, the resulting residue was purified by column chromatography on silica gel using hexane:ethyl acetate (9:1; 8:2; 7:3) mixtures.

*4.1.4. Experimental procedure for the synthesis of compounds **27–39***

Zn powder (147 eq.) was added to a solution of the corresponding nitrotetrazole derivative (1 eq.) in glacial AcOH (32.6 mL/mmol). The reaction mixture was vigorously stirred for 1 h at room temperature preserved from light. Next, the reaction mixture was filtered over Celite and the filtration residue was thoroughly washed with ethyl acetate. The filtrate was neutralized using an aqueous saturated solution of $NaHCO_3$ and Na_2CO_3 until basic pH (10–11). The aqueous phase was extracted with ethyl acetate (3 × 10 mL) and the collected organic phases were washed with brine and dried over anhydrous $MgSO_4$. After solvent elimination under vacuum, the residue was purified by column chromatography on silica gel using a hexane:ethyl acetate (1:1) mixture.

*4.1.5. Characterization of compounds **1–39***

3-(1-Benzyl-1*H*-1,2,3-triazol-4-yl)aniline (1): mass = 311 mg; yield = 20 %; m.p. = 144–146 °C (orange solid). IR ν_{max} 3309.9, 3205.5, 3004.2, 2836.5, 1652.3, 1613.9, 1494.7, 1248.7 cm-^{1}. NMR ^{1}H (400 MHz, DMSO-d_6) δ = 8.45 (s, 1H), 7.42–7.32 (m, 5H), 7.11 (apparent t, 1H), 7.06 (t, J = 8.0, 1H), 6.95 (dt, J = 7.6, 1 Hz, 1H), 6.53 (ddd, J = 8, 2.4, 1.2 Hz, 1H) 5.62 (s, 2H), 5.14 (broad s, 2H) ppm. NMR ^{13}C (100 MHz, DMSO-d_6) δ = 149.0 (C), 147.3 (C), 136.1 (C), 131.1 (C), 129.3 (CH), 128.7 (CH), 128.1 (CH), 127.9 (CH), 121.0 (CH), 113.6 (CH), 113.0 (CH), 110.5 (s), 52.9 (CH_2) ppm. HR ESMS *m/z* 251.1291 (M + H)$^+$. Calculated for $C_{15}H_{14}N_4$: 251.1297.

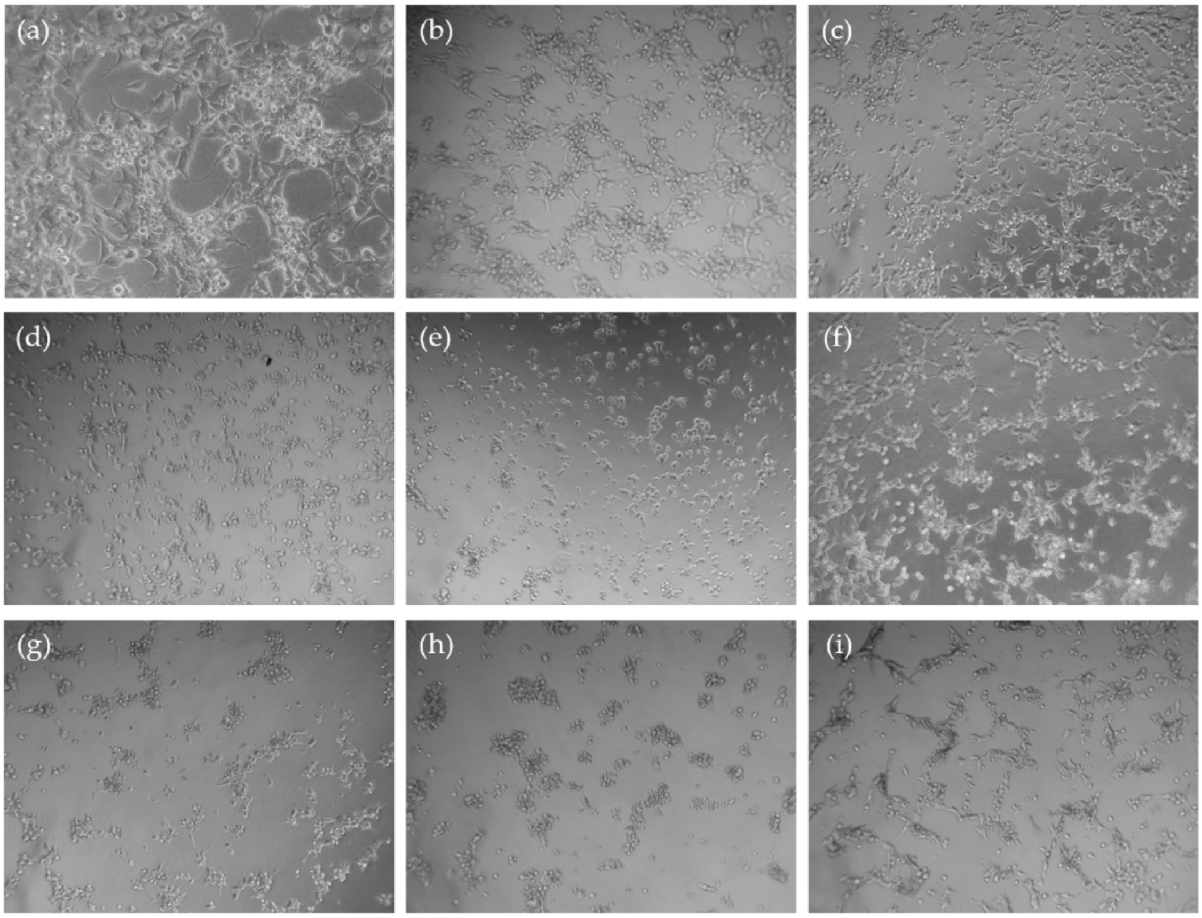

Fig. 6. Effect on vasculogenic mimicry after 24 h of (a) DMSO; (b) **10** (100 μM); (c) **13** (100 μM); (d) **34** (100 μM); (e) **35** (100 μM); (f) **36** (100 μM); (g) **37** (100 μM); (h) **38** (100 μM); (i) **39** (100 μM).

3-(1-(2-Methylbenzyl)-1*H*-1,2,3-triazol-4-yl)aniline (2): mass = 494 mg; yield = 63 %; m.p. = 132–134 °C (dark brown solid). IR ν_{max} 3309.9, 3205.5, 3004.2, 2836.5, 1652.3, 1613.9, 1494.7, 1248.7 cm-$^{1.}$ NMR ^{1}H (400 MHz, DMSO-d_6) δ = 8.33 (s, 1H), 7.28–7.18 (m, 3H), 7.13–7.08 (m, 2H), 7.05 (apparent t, 1H), 6.96 (t, J = 8 Hz, 1H), 6.93 (dt, J = 7.6, 1 Hz, 1H), 6.52 (ddd, J = 8, 2.4, 1.2 Hz, 1H), 5.62 (s, 2H), 5.13 (s, 2H), 2.34 (s, 3H) ppm. NMR ^{13}C (100 MHz, DMSO-d_6) δ = 149.0 (C), 147.2 (C), 136.2 (C), 134.2 (C), 131.1 (C), 130.4 (CH), 129.3 (CH), 128.6 (CH), 128.3 (CH), 126.3 (CH), 121.0 (CH), 113.6 (CH), 113.0 (CH), 110.5 (CH), 51.0 (CH_2), 18.6 (CH_3) ppm. HR ESMS *m/z* 265.1447 $(M + H)^+$. Calculated for $C_{16}H_{16}N_4$: 265.1453.

3-(1-(3-Methylbenzyl)-1*H*-1,2,3-triazol-4-yl)aniline (3): mass = 559 mg; yield = 62 %; m.p. = 107–109 °C (light brown solid). IR ν_{max} 3309.9, 3205.5, 3004.2, 2836.5, 1652.3, 1613.9, 1494.7, 1248.7 cm-^{1}. NMR ^{1}H (400 MHz, DMSO-d_6) δ = 8.43 (s, 1H), 7.26 (t, J = 8 Hz, 1H), 7.18–7.12 (m, 3H), 7.11 (apparent t, 1H), 7.06 (t, J = 8 Hz, 1H), 6,94 (dt, J = 7.6, 1 Hz, 1H), 6.53 (ddd, J = 8, 2.4, 1.2 Hz, 1H), 5.56 (s, 2H), 5.15 (s, 2H), 2.29 (s, 3H) ppm. NMR ^{13}C (100 MHz, DMSO-d_6) δ = 149.0 (C), 147.3 (C), 138.0 (C), 136.0 (C), 131.1 (C), 129.3 (CH), 128.7 (CH), 128.7 (CH), 128.4 (CH), 125.0 (CH), 121.0 (CH), 113.6 (CH), 113.1 (CH), 110.5 (CH), 52.9 (CH_2), 20.9 (CH_3) ppm. HR ESMS *m/z* 265.1447 $(M + H)^+$. Calculated for $C_{16}H_{16}N_4$: 265.1453.

3-(1-(4-Methylbenzyl)-1*H*-1,2,3-triazol-4-yl)aniline (4): mass = 448 mg; yield = 76 %; m.p. = 139–141 °C (light brown solid). IR ν_{max} 3309.9, 3205.5, 3004.2, 2836.5, 1652.3, 1613.9, 1494.7, 1248.7 cm-^{1}. NMR ^{1}H (400 MHz, DMSO-d_6) δ = 8.40 (s, 1H), 7.22 (dd, J = 16, 8 Hz, 4H), 7.08 (apparent t, 1H), 7.05 (t, J = 7.8 Hz, 1H), 6.92 (dt, J = 7.6, 1 Hz, 1H), 6.51 (ddd, J = 8, 2.3, 1 Hz, 1H), 5.55 (s, 2H), 5.11 (s, 2H), 2.28 (s, 3H) ppm. NMR ^{13}C (100 MHz, DMSO-d_6) δ = 149.0 (C), 147.3 (C), 137.4 (C), 132.5 (C), 131.1 (C), 129.3 (CH), 129.2 (CH) 127.9 (CH), 120.9 (CH), 113.6 (CH), 113.0 (CH), 110.5 (CH), 52.7 (CH_2), 20.7 (CH_3) ppm. HR ESMS *m/z* 265.1448 $(M + H)^+$. Calculated for $C_{16}H_{16}N_4$: 265.1453.

3-(1-(2-Methoxybenzyl)-1*H*-1,2,3-triazol-4-yl)aniline (5): mass = 580 mg; yield = 55 %; m.p. = 121–123 °C (orange solid) IR ν_{max} 3309.9, 3205.5, 3004.2, 2836.5, 1652.3, 1613.9, 1494.7, 1248.7, 1213.6 cm-^{1}. NMR ^{1}H (400 MHz, DMSO-d_6) δ = 8.28 (s, 1H), 7.35 (td, J = 8, 1 Hz, 1H), 7.13 (dd, J = 7.6, 1.6 Hz, 1H), 7.08 (t, J = 2 Hz 1H), 7.07–7.03 (m, 2H), 6.95 (ddd, J = 7.6, 2, 1.2, 2H), 5.55 (s, 2H), 5.1 (broad s, 2H), 3.83 (s, 3H) ppm. NMR ^{13}C (100 MHz, DMSO-d_6) δ = 156.8 (C), 149.0 (C), 146.9 (C), 131.2 (C), 129.9 (CH), 129.4 (CH), 129.2 (CH), 123.5 (CH), 121.0 (CH), 120.5 (CH), 113.5 (C), 113.1 (CH), 111.2 (CH), 110.4 (CH), 55.5 (CH_3), 48.2 (CH_2) ppm. HR ESMS *m/z* 281.1403 $(M + H)^+$. Calculated for $C_{16}H_{16}N_4O$: 281.1402.

3-(1-(3-Methoxybenzyl)-1*H*-1,2,3-triazol-4-yl)aniline (6): mass = 290 mg; yield = 59 %; m.p. = 115–116 °C (dark brown solid). IR ν_{max} 3309.9, 3205.5, 3004.2, 2836.5, 1652.3, 1613.9, 1494.7, 1248.7, 1213.6 cm-^{1}. NMR ^{1}H (400 MHz, DMSO-d_6) δ = 8.44 (s, 1H), 7.30 (t, J = 7.9 Hz, 1H), 7.10 (apparent t, 1H), 7.06 (t, J = 7.8 Hz, 1H), 6.95–6.87 (m, 4H), 6.52 (ddd, J = 8.0, 2.3, 1.0 Hz, 1H), 5.57 (s, 2H), 5.18 (broad s, 2H), 3.74 (s, 3H) ppm. NMR ^{13}C (100 MHz, DMSO-d_6) δ = 159.5 (C), 148.8 (C), 147.3 (C), 137.5 (C), 131.1 (C), 129.9 (CH), 129.3 (CH), 121.1 (CH), 120.0 (CH), 113.7 (CH), 113.6 (CH), 113.5 (CH), 113.1 (CH), 110.5 (CH), 55.1 (CH_2), 52.8 (CH_3) ppm. HR ESMS *m/z* 281.1398 $(M + H)^+$. Calculated for $C_{16}H_{16}N_4O$: 281.1402.

3-(1-(4-Methoxybenzyl)-1*H*-1,2,3-triazol-4-yl)aniline (7): mass = 495 mg; yield = 69 %; m.p. = 112–114 °C (orange solid). IR ν_{max} 3309.9, 3205.5, 3004.2, 2836.5, 1652.3, 1613.9, 1494.7, 1248.7,

1213.6 cm-1. NMR ^{1}H (400 MHz, DMSO-d_6) δ = 8.38 (s, 1H), 7.32 (dd, J = 7.9, 1.2 Hz, 2H), 7.08 (apparent t, 1H), 7.05 (t, J = 7.8 Hz, 1H), 6.96–6.90 (m, 3H), 6.51 (ddd, J = 8, 2.3, 1 Hz, 1H), 5.52 (s, 2H), 5.11 (broad s, 2H), 3.74 (s, 3H) ppm. NMR ^{13}C (100 MHz, DMSO-d_6) δ = 159.0 (C), 148.9 (C), 147.2 (C), 131.0 (C), 129.4 (CH), 129.2 (CH), 127.9 (C), 120.6 (CH), 114.0 (CH), 113.5 (CH), 112.9 (CH), 110.4 (CH), 55.0 (CH_2), 52.4 (CH_3) ppm. HR ESMS *m/z* 281.1399 $(M + H)^+$. Calculated for $C_{16}H_{16}N_4O$: 281.1402.

3-(1-(2-Bromobenzyl)-1*H*-1,2,3-triazol-4-yl)aniline (8): mass = 80 mg; yield = 38 %; m.p. = 117–118 °C (dark brown solid). IR ν_{max} 3309.9, 3205.5, 3004.2, 2836.5, 1652.3, 1613.9, 1494.7, 1248.7, 588.2 cm-1. NMR ^{1}H (400 MHz, DMSO-d_6) δ = 8.40 (s, 1H), 7.70 (dd, J = 7.9, 1.2 Hz, 1H), 7.42 (td, J = 7.5, 1.2 Hz, 1H), 7.32 (td, J = 7.7, 1.7 Hz, 1H), 7.19 (dd, J = 7.6, 1.7 Hz, 1H), 7.10 (apparent t, 1H), 7.06 (t, J = 7.8 Hz, 1H), 6.95 (dt, J = 7.6, 1 Hz, 1H), 6.53 (ddd, J = 8, 2.3, 1 Hz, 1H), 5.70 (s, 2H), 5.16 (broad s, 2H) ppm. NMR ^{13}C (100 MHz, DMSO-d_6) δ = 149.0 (C), 147.1 (C), 134.9 (C), 132.9 (CH), 131.0 (C), 130.4 (CH), 129.3 (CH), 129.2 (CH), 128.3 (CH), 122.8 (C), 121.5 (CH), 113.7 (CH), 113.1 (CH), 110.5 (CH), 53.0 (CH_2) ppm. HR ESMS *m/z* 329.0396 $(M + H)^+$. Calculated for $C_{15}H_{13}BrN_4$: 329.0402.

3-(1-(3-Bromobenzyl)-1*H*-1,2,3-triazol-4-yl)aniline (9): mass = 398 mg; yield = 65 %; m.p. = 107–109 °C (light brown solid). IR ν_{max} 3309.9, 3205.5, 3004.2, 2836.5, 1652.3, 1613.9, 1494.7, 1248.7, 588.2 cm-1. NMR ^{1}H (400 MHz, DMSO-d_6) δ = 8.48 (s, 1H), 7.59–7.52 (m, 2H), 7.38.7.32 (m, 2H), 7.10 (apparent t, 1H), 7.06 (t, J = 7.8 Hz, 1H), 6.95 (dt, J = 7.6, 1 Hz, 1H), 6.53 (ddd, J = 8, 2.3, 1 Hz, 1H), 5.63 (s, 2H), 5.15 (broad s, 2H) ppm. NMR ^{13}C (100 MHz, DMSO-d_6) δ = 149.0 (C), 147.4 (C), 138.7 (C), 131.0 (CH), 130.9 (CH), 130.6 (CH), 129.3 (CH), 129.2 (CH), 127.0 (CH), 121.8 (C), 121.2 (CH), 113.6 (CH), 113.0 (CH), 110.5 (CH), 52.1 (CH_3) ppm. HR ESMS *m/z* 329.0395 $(M + H)^+$. Calculated for $C_{15}H_{13}BrN_4$: 329.0402.

3-(1-(4-Bromobenzyl)-1*H*-1,2,3-triazol-4-yl)aniline (10): mass = 100 mg; yield = 17 %; m.p. = 174–176 °C (orange solid). IR ν_{max} 3309.9, 3205.5, 3004.2, 2836.5, 1652.3, 1613.9, 1494.7, 1248.7, 588.2 cm-1. NMR ^{1}H (400 MHz, DMSO-d_6) δ = 8.44 (s, 1H), 7.64–7.53 (m, 2H), 7.34–7.24 (m, 2H), 7.10 (apparent t, 1H), 7.05 (t, J = 7.8 Hz, 1H), 6.92 (dt, J = 7.6, 1 Hz, 1H), 6.52 (ddd, J = 8, 2.3, 1 Hz, 1H), 5.60 (s, 2H), 5.13 (broad s, 2H) ppm. NMR ^{13}C (100 MHz, DMSO-d_6) δ = 149.0 (C), 147.4 (C), 135.5 (C), 131.7 (CH), 131.0 (C), 130.1 (CH), 129.3 (CH), 121.4 (CH), 121.1 (CH), 113.6 (CH), 113.0 (CH), 110.5 (CH), 52.2 (CH_2) ppm. HR ESMS *m/z* 329.0397 $(M + H)^+$. Calculated for $C_{15}H_{13}BrN_4$: 329.0402.

3-(1-(2-Chlorobenzyl)-1*H*-1,2,3-triazol-4-yl)aniline (11): mass = 523 mg; yield = 42 %; m.p. = 107–109 °C (dark brown solid). IR ν_{max} 3309.9, 3205.5, 3004.2, 2836.5, 1652.3, 1613.9, 1494.7, 1248.7, 746.4 cm-1. NMR ^{1}H (400 MHz, DMSO-d_6) δ = 8.41 (s, 1H), 7.53 (dd, J = 7.9, 1.2 Hz, 1H), 7.43–7.34 (m, 2H), 7.25 (dd, J = 7.3, 2 Hz, 1H), 7.10 (apparent t, 1H), 7.06 (t, J = 7.8 Hz, 1H), 6.91(dt, J = 7.6, 1 Hz, 1H), 6.52 (ddd, J = 8, 2.3, 1 Hz, 1H), 5.72 (s, 2H), 5.13 (broad s, 2H) ppm. NMR ^{13}C (100 MHz, DMSO-d_6) δ = 148.9 (C), 147.0 (C), 133.2 (C), 132.5 (C), 130.9 (C), 130.3 (CH), 130.1 (CH), 129.5 (CH), 129.2 (CH), 127.6 (CH), 121.3 (CH), 113.5 (CH), 113.0 (CH), 110.4 (CH), 50.5 (CH_2) ppm. HR ESMS *m/z* 285.0902 $(M + H)^+$. Calculated for $C_{15}H_{13}ClN_4$: 285.0907.

3-(1-(3-Chlorobenzyl)-1*H*-1,2,3-triazol-4-yl)aniline (12): mass = 184 mg; yield = 78 %; m.p. = 105–106 °C (dark brown solid). IR ν_{max} 3309.9, 3205.5, 3004.2, 2836.5, 1652.3, 1613.9, 1494.7, 1248.7, 746.4 cm-1. NMR ^{1}H (400 MHz, DMSO-d_6) δ = 8.48 (s, 1H), 7.45–7.39 (m, 3H), 7.32–7.28 (m, 1H), 7.10 (apparent t, 1H), 7.06 (t, J = 7.8 Hz, 1H), 6.91 (dt, J = 7.6, 1 Hz, 1H), 6.53 (ddd, J = 8, 2.3, 1 Hz, 1H), 5.64 (s, 2H), 5.15 (broad s, 2H) ppm. NMR ^{13}C (100 MHz, DMSO-d_6) δ = 149.0 (C), 147.4 (C), 138.5 (C), 133.3 (C), 131.0 (C), 130.7 (CH), 129.3 (CH), 128.1 (CH), 127.8 (CH), 126.6 (CH), 121.2 (CH), 113.7 (CH), 113.1 (CH), 110.5 (CH), 52.1 (CH_2) ppm. HR ESMS *m/z* 285.0901 $(M + H)^+$. Calculated for $C_{15}H_{13}ClN_4$: 285.0907.

3-(1-(4-Chlorobenzyl)-1*H*-1,2,3-triazol-4-yl)aniline (13): mass = 198 mg; yield = 20 %; m.p. = 151–152 °C (light brown solid). IR ν_{max} 3309.9, 3205.5, 3004.2, 2836.5, 1652.3, 1613.9, 1494.7, 1248.7, 746.4 cm-1. NMR ^{1}H (400 MHz, DMSO-d_6) δ = 8.44 (s, 1H), 7.48–7.41 (m, 2H), 7.40–7.34 (m, 2H), 7.10 (apparent t, 1H), 7.05 (t, J = 7.8 Hz, 1H), 6.92 (dt, J = 7.6, 1 Hz, 1H), 6.52 (ddd, J = 8, 2.3, 1 Hz, 1H), 5.63 (s, 2H), 5.13 (broad s, 2H) ppm. NMR ^{13}C (100 MHz, DMSO-d_6) δ = 149.0 (C), 147.4 (C), 135.1 (C), 132.8 (C), 131.0 (C), 129.8 (CH), 129.3 (CH), 128.8 (CH), 121.1 (CH), 113.6 (CH), 113.0 (CH), 110.5 (CH), 52.1 (CH_2) ppm. HR ESMS *m/z* 285.0903 $(M + H)^+$. Calculated for $C_{15}H_{13}ClN_4$: 285.0907.

2-Benzyl-5-(3-nitrophenyl)–2*H*-tetrazole (14): mass = 354 mg; yield = 65 %; m.p. = 102–103 °C (orange solid). IR ν_{max} 3004.2, 2836.5, 1652.3, 1613.9, 1523.7, 1494.7, 1248.7 cm-1. NMR ^{1}H (400 MHz, $CDCl_3$) δ = 8.77 (apparent s, 1H), 8.27 (dd, J = 8, 3 Hz, 1H), 8.09 (ddd, J = 8, 2, 1 Hz, 1H), 7.47 (t, J = 8 Hz, 1H), 7.28 (dd, J = 8, 2 Hz, 2H), 7.27–7.18 (m, 3H), 5.68 (s, 2H) ppm. NMR ^{13}C (100 MHz, $CDCl_3$) δ = 163.5 (C), 148.7 (C), 133.1 (C), 132.4 (CH), 130.0 (CH), 129.1 (C), 129.0 (2XCH), 128.5 (CH), 124.8 (CH), 121.7 (CH), 57.1 (CH_2) ppm. HR ESMS *m/z* 282.0991 $(M + H)^+$. Calculated for $C_{14}H_{12}N_4$: 282.0995.

2-(2-Methylbenzyl)-5-(3-nitrophenyl)–2*H*-tetrazole (15): mass = 98 mg; yield = 13 %; m.p. = 90–91 °C (dark brown solid). IR ν_{max} 3004.2, 2836.5, 1652.3, 1613.9, 1523.7, 1494.7, 1248.7 cm-1. NMR ^{1}H (400 MHz, $CDCl_3$) δ = 8.95 (apparent s, 1H), 8.46 (dd, J = 8, 3 Hz, 1H), 8.29 (ddd, J = 8, 2, 1 Hz, 1H), 7.65 (t, J = 8 Hz, 1H), 7.35 (d, J = 4 Hz, 1H), 7.33–7.23 (m, 3H), 5.87 (s, 2H), 2.50 (s, 3H) ppm. NMR ^{13}C (100 MHz, $CDCl_3$) δ = 163.4 (C), 148.7 (C), 137.1 (C), 132.6 (CH), 131.3 (C), 131.0 (CH), 130.1 (2XCH), 129.5 (CH), 129.2 (C), 126.7 (CH), 124.6 (CH), 121.8 (CH), 55.2 (CH_2), 19.6 (CH_3) ppm. HR ESMS *m/z* 296.1141 $(M + H)^+$. Calculated for $C_{15}H_{13}N_5O_2$: 296.1147.

2-(3-Methylbenzyl)-5-(3-nitrophenyl)–2*H*-tetrazole (16): mass = 312 mg; yield = 61 %; m.p. = 105–107 °C (light brown solid). IR ν_{max} 3004.2, 2836.5, 1652.3, 1613.9, 1523.7, 1494.7, 1248.7 cm-1. NMR ^{1}H (400 MHz, $CDCl_3$) δ = 8.97 (apparent s, 1H), 8.47 (dd, J = 8, 3 Hz, 1H), 8.29 (ddd, J = 8, 2, 1 Hz, 1H), 7.65 (t, J = 8 Hz, 1H), 7.32–7.18 (m, 4H), 5.81 (s, 2H), 2.37 (s, 3H) ppm. NMR ^{13}C (100 MHz, $CDCl_3$) δ = 163.5 (C), 148.7 (C), 139.0 (C), 133.0 (C), 132.6 (CH), 130.1 (CH), 130.0 (CH), 129.3 (C), 129.2 (CH), 129.1 (CH), 125.7 (CH), 124.7 (CH), 121.8 (CH), 57.3 (CH_2), 21.3 (CH_3) ppm. HR ESMS *m/z* 296.1143 $(M + H)^+$. Calculated for $C_{15}H_{13}N_5O_2$: 296.1147.

2-(4-Methylbenzyl)-5-(3-nitrophenyl)–2*H*-tetrazole (17): mass = 341 mg; yield = 67 %; m.p. = 99–100 °C (yellow solid). IR ν_{max} 3004.2, 2836.5, 1652.3, 1613.9, 1523.7, 1494.7, 1248.7 cm-1. NMR ^{1}H (400 MHz, $CDCl_3$) δ = 8.93 (apparent s, 1H), 8.42 (dd, J = 8, 3 Hz, 1H), 8.25 (ddd, J = 8, 2, 1 Hz, 1H), 7.65 (t, J = 8 Hz, 1H), 7.33 (d, J = 8H, 2H), 7.18 (d, J = 8 Hz, 2H), 5.77 (s, 2H), 2.32 (s, 3H) ppm. NMR ^{13}C (100 MHz, $CDCl_3$) δ = 163.5 (C), 148.7 (C), 139.1 (C), 132.5 (CH), 130.2 (C), 130.0 (CH), 129.8 (CH), 129.2 (C), 128.5 (CH), 124.7 (CH), 121.7 (CH), 56.9 (CH_2), 21.2 (CH_3) ppm. HR ESMS *m/z* 296.1143 $(M + H)^+$. Calculated for $C_{15}H_{13}N_5O_2$: 296.1147.

2-(2-Methoxybenzyl)-5-(3-nitrophenyl)–2*H*-tetrazole (18): mass = 258 mg; yield = 56 %; m.p. = 102–103 °C (orange solid). IR ν_{max} 3004.2, 2836.5, 1652.3, 1613.9, 1523.7, 1494.7, 1248.7, 1213.6 cm-1. NMR ^{1}H (400 MHz, $CDCl_3$) δ = 8.87 (apparent s, 1H), 8.38 (dd, J = 8, 3 Hz, 1H), 8.18 (ddd, J = 8, 2, 1 Hz, 1H), 7.55 (t, J = 8 Hz, 1H), 7.27 (td, 8, 1 Hz, 1H), 7.16 (dd, J = 8, 1 Hz, 1H), 6.91–6.83 (m, 2H), 5.78 (s, 2H), 3.77 (s, 3H) ppm. NMR ^{13}C (100 MHz, $CDCl_3$) δ = 163.3 (C), 157.4 (C), 148.7 (C), 132.6 (CH), 130.7 (CH), 130.3 (CH), 130.0 (CH), 129.4 (C), 125.0 (CH), 122.0 (CH), 121.5 (C), 120.8 (CH), 111.0 (CH), 55.7 (CH_3), 52.2 (CH_2) ppm. HR ESMS *m/z* 334.1093 $(M + H)^+$. Calculated for $C_{15}H_{13}N_5O_3$: 312.1097.

2-(3-Methoxybenzyl)-5-(3-nitrophenyl)–2*H*-tetrazole (19): mass = 127 mg; yield = 24 %; m.p. = 93–94 °C (yellow solid). IR ν_{max} 3004.2, 2836.5, 1652.3, 1613.9, 1523.7, 1494.7, 1248.7, 1213.6 cm-1. NMR ^{1}H (400 MHz, $CDCl_3$) δ = 8.82 (apparent s, 1H), 8.32 (dd, J = 8, 3 Hz, 1H), 8.14 (ddd, J = 8, 2, 1 Hz, 1H), 7.51 (t, J = 8 Hz, 1H), 7.17 (t, 8 Hz, 1H), 6.90–6.82 (m, 2H), 6.77 (dd, J = 8, 2 Hz, 1H), 5.67 (s, 2H), 3.67 (s, 3H) ppm. NMR ^{13}C (100 MHz, $CDCl_3$) δ = 163.5 (C), 160.1 (C), 148.6 (C),

134.4 (C), 132.5 (CH), 130.3 (CH), 130.0 (CH), 129.2 (C), 124.7 (CH), 121.7 (CH), 120.6 (CH), 114.5 (CH), 114.2 (CH), 57.0 (CH_2), 55.6 (CH_3) ppm. HR ESMS *m/z* 334.1096 $(M + H)^+$. Calculated for $C_{15}H_{13}N_5O_3$: 312.1097.

2-(4-Methoxybenzyl)-5-(3-nitrophenyl)–2*H*-tetrazole (20): mass = 197 mg; yield = 48 %; m.p. = 149–150 °C (yellow solid). IR ν_{max} 3004.2, 2836.5, 1652.3, 1613.9, 1523.7, 1494.7, 1248.7, 1213.6 cm-^{1}. NMR ^{1}H (400 MHz, $CDCl_3$) δ = 8.95 (apparent s, 1H), 8.36 (dd, *J* = 8, 3 Hz, 1H), 8.28 (ddd, *J* = 8, 2, 1 Hz, 1H), 7.65 (t, *J* = 8 Hz, 1H), 7.40 (d, *J* = 8 Hz, 2H), 6.91 (d, *J* = 8 Hz, 2H), 5.75 (s, 2H), 3.79 (s, 3H) ppm. NMR ^{13}C (100 MHz, $CDCl_3$) δ = 163.6 (C), 160.3 (C), 148.7 (C), 132.6 (C), 130.3 (CH), 129.3 (C), 125.1 (C), 124.8 (CH), 122.0 (CH), 114.5 (CH), 114.2 (CH), 56.8 (CH_2), 55.5 (CH_3) ppm. HR ESMS *m/z* 334.1089 $(M + H)^+$. Calculated for $C_{15}H_{13}N_5O_3$: 312.1097.

2-(2-Bromobenzyl)-5-(3-nitrophenyl)–2*H*-tetrazole (21): mass = 245 mg; yield = 30 %; m.p. = 104–106 °C (light brown solid). IR ν_{max} 3004.2, 2836.5, 1652.3, 1613.9, 1523.7, 1494.7, 1248.7, 588.2 cm-^{1}. NMR ^{1}H (400 MHz, $CDCl_3$) δ = 8.97 (apparent s, 1H), 8.48 (dd, *J* = 8, 3 Hz, 1H), 8.31 (ddd, *J* = 8, 2, 1 Hz, 1H), 7.67 (t, *J* = 8 Hz, 1H), 7.65 (dd, *J* = 8, 2 Hz, 1H), 7.35 (td, *J* = 8, 2 Hz, 1H), 7.29–7.23 (m, 2H), 5.99 (s, 2H) ppm. NMR ^{13}C (100 MHz, $CDCl_3$) δ = 163.7 (C), 148.8 (C), 133.5 (CH), 132.7 (CH), 132.6 (C), 130.9 (CH), 130.6 (CH), 130.1 (CH), 129.2 (C), 128.3 (CH), 125.1 (CH), 123.8 (C), 122.2 (CH), 56.9 (CH_2) ppm. HR ESMS *m/z* 360.0092 $(M + H)^+$. Calculated for $C_{14}H_{10}BrN_5O_2$: 360.0096.

2-(3-Bromobenzyl)-5-(3-nitrophenyl)–2*H*-tetrazole (22): mass = 106 mg; yield = 17 %; m.p. = 119–121 °C (light brown solid). IR ν_{max} 3004.2, 2836.5, 1652.3, 1613.9, 1523.7, 1494.7, 1248.7, 588.2 cm-^{1}. NMR ^{1}H (400 MHz, $CDCl_3$) δ = 8.95 (apparent s, 1H), 8.46 (dd, *J* = 8, 3 Hz, 1H), 8.29 (ddd, *J* = 8, 2, 1 Hz, 1H), 7.65 (t, *J* = 8 Hz, 1H), 7.57 (apparent s, 1H), 7.50 (d, *J* = 8 Hz, 1H), 7.37 (d, *J* = 8 Hz, 1H), 7.26 (t, *J* = 8 Hz, 1H), 5.77 (s, 2H) ppm. NMR ^{13}C (100 MHz, $CDCl_3$) δ = 163.7 (C), 148.8 (C), 135.1 (C), 132.6 (CH), 132.5 (CH), 131.7 (CH), 130.8 (CH), 130.2 (CH), 129.1 (C), 127.3 (CH), 125.0 (CH), 123.2 (C), 122.0 (CH), 56.4 (CH_2) ppm. HR ESMS *m/z* 360.0104 $(M + H)^+$. Calculated for $C_{14}H_{10}BrN_5O_2$: 360.0096.

2-(4-Bromobenzyl)-5-(3-nitrophenyl)–2*H*-tetrazole (23): mass = 331 mg; yield = 58 %; m.p. = 114–116 °C (yellow solid). IR ν_{max} 3004.2, 2836.5, 1652.3, 1613.9, 1523.7, 1494.7, 1248.7, 588.2 cm-^{1}. NMR ^{1}H (400 MHz, $CDCl_3$) δ = 8.96 (apparent s, 1H), 8.46 (dd, *J* = 8, 3 Hz, 1H), 8.31 (ddd, *J* = 8, 2, 1 Hz, 1H), 7.67 (t, *J* = 8 Hz, 1H), 7.54 (d, *J* = 8 Hz, 2H), 7.33 (d, *J* = 8 Hz, 2H), 5.76 (s, 2H) ppm. NMR ^{13}C (100 MHz, $CDCl_3$) δ = 163.9 (C), 148.7 (C), 132.7 (CH), 132.5 (CH), 132.0 (C), 130.4 (CH), 130.2 (CH), 129.1 (C), 125.1 (CH), 123.7 (C), 122.1 (CH), 56.6 (CH_2) ppm. HR ESMS *m/z* 360.0091 $(M + H)^+$. Calculated for $C_{14}H_{10}BrN_5O_2$: 360.0096.

2-(2-Chlorobenzyl)-5-(3-nitrophenyl)–2*H*-tetrazole (24): mass = 240 mg; yield = 48 %; m.p. = 105–107 °C (yellow solid). IR ν_{max} 3004.2, 2836.5, 1652.3, 1613.9, 1523.7, 1494.7, 1248.7, 746.4 cm-^{1}. NMR ^{1}H (400 MHz, $CDCl_3$) δ = 8.87 (apparent s, 1H), 8.40 (dd, *J* = 8, 3 Hz, 1H), 8.22 (ddd, *J* = 8, 2, 1 Hz, 1H), 7.60 (t, *J* = 8 Hz, 1H), 7.38 (d, *J* = 8 Hz, 1H), 7.31–7.24 (m, 3H), 5.94 (s, 2H) ppm. NMR ^{13}C (100 MHz, $CDCl_3$) δ = 163.4 (C), 148.5 (C), 133.7 (C), 132.5 (CH), 130.7 (C), 130.6 (CH), 130.5 (CH), 130.0 (CH), 129.9 (CH), 128.9 (C), 127.4 (CH), 124.7 (CH), 121.7 (CH), 54.4 (CH_2) ppm. HR ESMS *m/z* 316.0596 $(M + H)^+$. Calculated for $C_{14}H_{10}ClN_5O_2$: 316.0601.

2-(3-Chlorobenzyl)-5-(3-nitrophenyl)–2*H*-tetrazole (25): mass = 388 mg; yield = 66 %; m.p. = 102–103 °C (light brown solid). IR ν_{max} 3004.2, 2836.5, 1652.3, 1613.9, 1523.7, 1494.7, 1248.7, 746.4 cm-^{1}. NMR ^{1}H (400 MHz, $CDCl_3$) δ = 8.94 (apparent s, 1H), 8.44 (dd, *J* = 8, 3 Hz, 1H), 8.28 (ddd, *J* = 8, 2, 1 Hz, 1H), 7.65 (t, *J* = 8 Hz, 1H), 7.42 (apparent s, 1H), 7.35–7.30 (m, 3H), 5.80 (s, 2H) ppm. NMR ^{13}C (100 MHz, $CDCl_3$) δ = 163.7 (C), 148.6 (C), 135.0 (C), 134.8 (C), 132.6 (CH), 130.5 (CH), 130.1 (CH), 129.5 (CH), 129.0 (C), 128.7 (CH), 126.7 (CH), 125.0 (CH), 121.8 (CH), 56.4 (CH_2) ppm. HR ESMS *m/z* 316.0599 $(M + H)^+$. Calculated for $C_{14}H_{10}ClN_5O_2$: 316.0601.

2-(4-Chlorobenzyl)-5-(3-nitrophenyl)–2*H*-tetrazole (26): mass = 368 mg; yield = 72 %; m.p. = 111–113 °C (light brown solid). IR ν_{max} 3004.2, 2836.5, 1652.3, 1613.9, 1523.7, 1494.7, 1248.7, 746.4 cm-^{1}. NMR ^{1}H (400 MHz, $CDCl_3$) δ = 8.96 (apparent s, 1H), 8.47 (dd, *J* = 8, 3 Hz, 1H), 8.30 (ddd, *J* = 8, 2, 1 Hz, 1H), 7.66 (t, *J* = 8 Hz, 1H), 7.41–7.35 (m, 4H), 5.80 (s, 2H) ppm. NMR ^{13}C (100 MHz, $CDCl_3$) δ = 163.8 (C), 148.7 (C), 135.5 (C), 132.6 (CH), 131.4 (C), 130.2 (CH), 130.1 (CH), 129.5 (CH), 129.1 (C), 125.1 (CH), 121.9 (CH), 56.5 (CH_2) ppm. HR ESMS *m/z* 316.0594 $(M + H)^+$. Calculated for $C_{14}H_{10}ClN_5O_2$: 316.0601.

3-(2-Benzyl-2*H*-tetrazol-5-yl)aniline (27): mass = 211 mg; yield = 77 %; m.p. = 94–95 °C (light brown solid). IR ν_{max} 3309.9, 3205.5, 3004.2, 2836.5, 1652.3, 1613.9, 1494.7, 1248.7 cm-^{1}. NMR ^{1}H (400 MHz, $CDCl_3$) δ = 7.42 (d, *J* = 8 Hz, 1H), 7.36 (apparent s, 1H), 7.30–7.20 (m, 5H), 7.11 (t, *J* = 8 Hz, 1H), 6.63 (dd, *J* = 8, 2 Hz, 1H), 5.65 (s, 2H), 3.70 (broad s, 2H) ppm. NMR ^{13}C (100 MHz, $CDCl_3$) δ = 165.5 (C), 146.9 (C), 133.4 (C), 129.9 (CH), 128.9 (CH), 128.8 (CH), 128.3 (CH), 128.2 (C), 117.1 (CH), 117.0 (CH), 113.2 (CH), 56.7 (CH_2) ppm. HR ESMS *m/z* 252.1247 $(M + H)^+$. Calculated for $C_{14}H_{13}N_5$: 252.1249.

3-(2-(2-Methylbenzyl)–2*H*-tetrazol-5-yl)aniline (28): mass = 64 mg; yield = 76 %; m.p. = 95–96 °C (orange solid). IR ν_{max} 3309.9, 3205.5, 3004.2, 2836.5, 1652.3, 1613.9, 1494.7, 1248.7 cm-^{1}. NMR ^{1}H (400 MHz, DMSO-d_6) δ = 7.30–7.20 (m, 5H), 7.18–7.12 (m, 2H), 6.70–6.64 (m, 1H), 5.95 (s, 2H), 5.34 (broad s, 2H), 2.35 (s, 3H) ppm. NMR ^{13}C (100 MHz, DMSO-d_6) δ = 164.8 (C), 149.3 (C), 136.8 (C), 132.2 (C), 130.5 (CH), 129.6 (CH), 129.5 (CH), 128.8 (CH), 127.2 (C), 126.3 (CH), 115.8 (CH), 113.6 (CH), 111.3 (CH), 54.3 (CH_2), 18.6 (CH_3) ppm. HR ESMS *m/z* 266.1398 $(M + H)^+$. Calculated for $C_{15}H_{15}N_5$: 266.1406.

3-(2-(3-Methylbenzyl)–2*H*-tetrazol-5-yl)aniline (29): mass = 196 mg; yield = 76 %; m.p. = 97–98 °C (orange solid). IR ν_{max} 3309.9, 3205.5, 3004.2, 2836.5, 1652.3, 1613.9, 1494.7, 1248.7 cm-^{1}. NMR ^{1}H (400 MHz, DMSO-d_6) δ = 7.31–7.26 (m, 2H), 7.22–7.12 (m, 5H), 6.68 (dt, *J* = 8, 1 Hz, 1H), 5.90 (s, 2H), 5.35 (broad s, 2H), 2.29 (s, 3H) ppm. NMR ^{13}C (100 MHz, DMSO-d_6) δ = 164.9 (C), 149.3 (C), 138.2 (C), 134.1 (C), 129.6 (CH), 129.2 (CH), 128.8 (CH), 128.7 (CH), 127.3 (C), 125.3 (CH), 115.8 (CH), 113.5 (CH), 111.2 (CH), 56.0 (CH_2), 20.8 (CH_3) ppm. HR ESMS *m/z* 266.1400 $(M + H)^+$. Calculated for $C_{15}H_{15}N_5$: 266.1406.

3-(2-(4-Methylbenzyl)–2*H*-tetrazol-5-yl)aniline (30): mass = 287 mg; yield = 76 %; m.p. = 102–103 °C (light brown solid). IR ν_{max} 3309.9, 3205.5, 3004.2, 2836.5, 1652.3, 1613.9, 1494.7, 1248.7 cm-^{1}. NMR ^{1}H (400 MHz, DMSO-d_6) δ = 7.31–7.26 (m, 3H), 7.21 (d, *J* = 8 Hz, 2H), 7.18–7.12 (m, 2H), 6.70–6.65 (m, 1H), 5.89 (s, 2H), 5.33 (broad s, 2H), 2.28 (s, 3H) ppm. NMR ^{13}C (100 MHz, DMSO-d_6) δ = 164.9 (C), 149.3 (C), 138.0 (C), 131.2 (C), 129.6 (CH), 129.4 (CH), 128.3 (CH), 127.3 (C), 115.8 (CH), 113.5 (CH), 111.3 (CH), 55.7 (CH_2), 20.6 (CH_3) ppm. HR ESMS *m/z* 266.1403 $(M + H)^+$. Calculated for $C_{15}H_{15}N_5$: 266.1406.

3-(2-(2-Methoxybenzyl)–2*H*-tetrazol-5-yl)aniline (31): mass = 188 mg; yield = 65 %; m.p. = 108–109 °C (yellow solid). IR ν_{max} 3309.9, 3205.5, 3004.2, 2836.5, 1652.3, 1613.9, 1494.7, 1248.7, 1213.6 cm-^{1}. NMR ^{1}H (400 MHz, DMSO-d_6) δ = 7.38 (td, *J* = 8, 2 Hz, 1H), 7.27–7.25 (m, 2H), 7.17–7.13 (m, 2H), 7.07 (d, *J* = 8 Hz, 1H), 6.97 (td, *J* = 8, 2 Hz, 1H), 6.70–6.64 (m, 1H), 5.85 (s, 2H), 5.35 (broad s, 2H), 3.77 (s, 3H) ppm. NMR ^{13}C (100 MHz, DMSO-d_6) δ = 164.6 (C), 157.1 (C), 149.2 (C), 130.4 (CH), 130.3 (CH), 129.6 (CH), 127.3 (C), 121.7 (C), 120.5 (CH), 115.7 (CH), 113.6 (CH), 111.3 (CH), 111.2 (CH), 55.7 (CH_3), 51.5 (CH_2) ppm. HR ESMS *m/z* 282.1352 $(M + H)^+$. Calculated for $C_{15}H_{15}N_5O$: 282.1355.

3-(2-(3-Methoxybenzyl)–2*H*-tetrazol-5-yl)aniline (32): mass = 81 mg; yield = 53 %, m.p. = 107–108 °C (yellow solid). IR ν_{max} 3309.9, 3205.5, 3004.2, 2836.5, 1652.3, 1613.9, 1494.7, 1248.7, 1213.6 cm-^{1}. NMR ^{1}H (400 MHz, DMSO-d_6) δ = 7.32 (t, *J* = 8 Hz, 2H), 7.23–7.15 (m, 2H), 6.98–6.96 (m, 1H), 6.95–6.90 (m, 2H), 6.70 (dt, *J* = 8, 1 Hz), 5.93 (s, 2H), 3.75 (s, 3H) ppm. NMR ^{13}C (100 MHz, DMSO-d_6) δ = 164.8 (C), 159.4 (C), 148.2 (C), 135.5 (C), 130.0 (CH), 129.7 (CH), 127.2 (C), 120.2 (CH), 116.5 (CH), 114.4 (CH), 114.0 (CH), 113.9 (CH), 112.0

(CH), 55.6 (CH_2), 55.2 (CH_3) ppm. HR ESMS *m/z* 282.1348 $(M + H)^+$. Calculated for $C_{15}H_{15}N_5O$: 282.1355.

3-(2-(4-Methoxybenzyl)–2*H*-tetrazol-5-yl)aniline (33): mass = 102 mg; yield = 65 %, m.p. = 104–105 °C (light brown solid). IR ν_{max} 3309.9, 3205.5, 3004.2, 2836.5, 1652.3, 1613.9, 1494.7, 1248.7, 1213.6 cm-^{1}. NMR ^{1}H (400 MHz, DMSO-d_6) δ = 7.37 (d, J = 8 Hz, 2H), 7.29–7.26 (m, 1H), 7.18–7.12 (m, 2H), 6.95 (d, J = 8 Hz, 2H), 6.67 (dt, J = 8, 1 Hz, 1H), 5.86 (s, 2H), 5.35 (broad s, 2H), 3.74 (s, 3H) ppm. NMR ^{13}C (100 MHz, DMSO-d_6) δ = 164.8 (C), 159.4 (C), 149.3 (C), 130.0 (CH), 129.6 (CH), 127.3 (C), 126.1 (C), 115.8 (CH), 114.2 (CH), 113.6 (CH), 111.4 (CH), 55.6 (CH_2), 55.2 (CH_3) ppm. HR ESMS *m/z* 282.1346 $(M + H)^+$. Calculated for $C_{15}H_{15}N_5O$: 282.1355.

3-(2-(2-Bromobenzyl)–2*H*-tetrazol-5-yl)aniline (34): mass = 170 mg; yield = 72 %; m.p. = 109–111 °C (orange solid). IR ν_{max} 3309.9, 3205.5, 3004.2, 2836.5, 1652.3, 1613.9, 1494.7, 1248.7, 588.2 cm-^{1}. NMR ^{1}H (400 MHz, DMSO-d_6) δ = 7.72 (d, J = 8 Hz, 1H), 7.47 (d, J = 4 Hz, 2H), 7.40–7.33 (m, 1H), 7.27–7.24 (m, 1H), 7.17–7.13 (m, 2H), 6.70–6.66 (m, 1H), 6.03 (s, 2H), 5.37 (broad s, 2H) ppm. NMR ^{13}C (100 MHz, DMSO-d_6) δ = 164.8 (C), 149.3 (C), 133.0 (CH), 131.8 (CH), 130.9 (CH), 129.6 (CH), 128.7 (C), 128.2 (CH), 127.2 (C), 123.5 (C), 115.8 (CH), 113.6 (CH), 111.3 (CH), 56.2 (CH_2) ppm. HR ESMS *m/z* 330.0345 $(M + H)^+$. Calculated for $C_{14}H_{12}BrN_5$: 330.0354.

3-(2-(3-Bromobenzyl)–2*H*-tetrazol-5-yl)aniline (35): mass = 58 mg; yield = 62 %; m.p. = 104–106 °C (yellow solid). IR ν_{max} 3309.9, 3205.5, 3004.2, 2836.5, 1652.3, 1613.9, 1494.7, 1248.7, 588.2 cm-^{1}. NMR ^{1}H (400 MHz, DMSO-d_6) δ = 7.65 (s, 1H), 7.61–7.56 (m, 1H), 7.40–7.35 (m, 2H), 7.29–7.26 (m, 1H), 7.18–7.14 (m, 2H), 6.68 (dt, J = 8, 1 Hz, 1H), 5.99 (s, 2H), 5.37 (broad s, 2H) ppm. NMR ^{13}C (100 MHz, DMSO-d_6) δ = 165.1 (C), 149.4 (C), 136.6 (C), 131.5 (CH), 131.3 (CH), 131.2 (CH), 129.7 (CH), 127.5 (CH), 127.3 (C), 121.8 (C), 115.9 (CH), 113.6 (CH), 111.3 (CH), 55.2 (CH_2) ppm. HR ESMS *m/z* 330.0359 $(M + H)^+$. Calculated for $C_{14}H_{12}BrN_5$: 330.0354.

3-(2-(4-Bromobenzyl)–2*H*-tetrazol-5-yl)aniline (36): mass = 219 mg; yield = 78 %; m.p. = 113–115 °C (orange solid). IR ν_{max} 3309.9, 3205.5, 3004.2, 2836.5, 1652.3, 1613.9, 1494.7, 1248.7, 588.2 cm-^{1}. NMR ^{1}H (400 MHz, DMSO-d_6) δ = 7.61 (d, J = 8 Hz, 2H), 7.36 (d, J = 8 Hz, 2H), 7.28–7.26 (m, 1H), 7.17–7.13 (m, 2H), 6.68 (dt, J = 8, 1 Hz, 1H), 5.96 (s, 2H), 5.37 (broad s, 2H) ppm. NMR ^{13}C (100 MHz, DMSO-d_6) δ = 165.5 (C), 149.7 (C), 134.0 (C), 132.3 (CH), 131.0 (CH), 130.1 (CH), 127.6 (C), 122.4 (C), 116.3 (CH), 114.2 (CH), 111.7 (CH), 55.6 (CH_2) ppm. HR ESMS *m/z* 330.0346 $(M + H)^+$. Calculated for $C_{14}H_{12}BrN_5$: 330.0354.

3-(2-(2-Chlorobenzyl)–2*H*-tetrazol-5-yl)aniline (37): mass = 183 mg; yield = 80 %; m.p. = 95–97 °C (orange solid). IR ν_{max} 3309.9, 3205.5, 3004.2, 2836.5, 1652.3, 1613.9, 1494.7, 1248.7, 746.4 cm-^{1}. NMR ^{1}H (400 MHz, $CDCl_3$) δ = 7.55 (dt, J = 8, 2 Hz, 1H), 7.50 (t, J = 4 Hz, 1H), 7.45 (dd, J = 8, 2 Hz, 1H), 7.31 (td, J = 8, 4 Hz, 1H), 7.26 (t, J = 8 Hz, 2H), 7.18 (dd, J = 8, 2 Hz, 1H), 6.77 (dd, J = 8, 2 Hz, 1H), 5.95 (s, 2H), 3.68 (broad s, 2H) ppm. NMR ^{13}C (100 MHz, $CDCl_3$) δ = 165.6 (C), 147.0 (C), 133.6 (C), 131.3 (C), 130.3 (CH), 130.1 (CH), 129.8 (CH), 129.7 (CH), 128.2 (C), 127.3 (CH), 117.0 (CH), 116.9 (CH) 113.2 (CH), 54.0 (CH_2) ppm. HR ESMS *m/z* 286.0857 $(M + H)^+$. Calculated for $C_{14}H_{12}ClN_5$: 286.0859.

3-(2-(3-Chlorobenzyl)–2*H*-tetrazol-5-yl)aniline (38): mass = 208 mg; yield = 78 %; m.p. = 80–83 °C (light brown solid). IR ν_{max} 3309.9, 3205.5, 3004.2, 2836.5, 1652.3, 1613.9, 1494.7, 1248.7, 746.4 cm-^{1}. NMR ^{1}H (400 MHz, DMSO-d_6) δ = 7.53–7.51 (m, 1H), 7.47–7.42 (m, 2H), 7.37–7.32 (m, 1H), 7.30–7.27 (m, 1H), 7.20–7.13 (m, 2H), 7.68 (dt, J = 8, 2 Hz, 1H), 5.98 (s, 2H), 5.34 (broad s, 2H) ppm. NMR ^{13}C (100 MHz, DMSO-d_6) δ = 165.1 (C), 149.3 (C), 136.4 (C), 133.3 (C), 130.7 (CH), 129.6 (CH), 128.6 (CH), 128.2 (CH), 127.2 (C), 127.0 (CH), 115.9 (CH), 113.6 (CH), 111.2 (CH), 55.1 (CH_2) ppm. HR ESMS *m/z* 286.0853 $(M + H)^+$. Calculated for $C_{14}H_{12}ClN_5$: 286.0859.

3-(2-(4-Chlorobenzyl)–2*H*-tetrazol-5-yl)aniline (39): mass = 230 mg; yield = 76 %; m.p. = 103–104 °C (light brown solid). IR ν_{max} 3309.9, 3205.5, 3004.2, 2836.5, 1652.3, 1613.9, 1494.7, 1248.7, 746.4 cm-^{1}. NMR ^{1}H (400 MHz, DMSO-d_6) δ = 7.47 (d, J = 8 Hz, 2H), 7.44 (d, J = 8 Hz, 2H), 7.31–7.27 (m, 1H), 7.20–7.13 (m, 2H), 6.68 (dt, J = 8, 2 Hz, 1H), 5.97 (s, 2H), 5.34 (broad s, 2H) ppm. NMR ^{13}C (100 MHz, DMSO-d_6) δ = 165.1 (C), 149.3 (C), 133.3 (C), 133.1 (C), 130.3 (CH), 129.6 (CH), 128.8 (CH), 127.2 (C), 115.8 (CH), 113.6 (CH), 111.2 (CH), 55.2 (CH_2) ppm. HR ESMS *m/z* 286.0856 $(M + H)^+$. Calculated for $C_{14}H_{12}ClN_5$: 286.0859.

4.2. Biological studies

4.2.1. Cell culture

Cell culture media were purchased from Gibco (Grand Island, NY). Fetal bovine serum (FBS) was obtained from Harlan-Seralab (Belton, U. K.). Supplements and other chemicals not listed in this section were obtained from Sigma Chemical Co. (St. Louis, MO). Plastics for cell culture were supplied by Thermo Scientific BioLite. All tested compounds were dissolved in DMSO at a concentration of 20 mM and stored at − 20 °C until use.

HT-29, A-549, MCF-7 and HEK-293 cell lines were maintained in Dulbecco's modified Eagle's medium (DMEM) containing glucose (1 g/L), glutamine (2 mM), penicillin (50 μg/mL), streptomycin (50 μg/mL), and amphotericin B (1.25 μg/mL), supplemented with 10 % FBS. For the HMEC-1 cell line, it was used Dulbecco's modified Eagle medium (DMEM)/Low glucose containing glutamine (2 mM), penicillin (50 μg/mL), streptomycin (50 μg/mL), and amphotericin B (1.25 μg/mL), supplemented with 10% FBS. For the development of the antiangiogenesis test, the HMEC-1 cells were seeded on matrigel in EGM-2MV Medium supplemented with EGM-2MV SingleQuots (Lonza, CA, USA).

4.2.2. Cell proliferation assay

5×10^3 cells per well were incubated in 96-well plates with serial dilutions of the tested compounds in a total volume of 100 μL of their growth media. 3-(4,5-dimethylthiazol-2-yl)-2,5-diphenyltetrazolium bromide (MTT; Sigma Chemical Co.) dye reduction assay in 96-well microplates was used. 10 μL of MTT (5 mg/mL in phosphate-buffered saline, PBS) was added to each well after 2 days of incubation (37 °C, 5% CO_2 in a humid atmosphere). The plate was incubated for a further 3 h (37 °C). After that, the supernatant was discarded and 100 μL of DMSO were added in order to dissolve formazan crystals. The absorbance was read at 550 nm by spectro-photometry. For all concentrations of compound, cell viability was expressed as the percentage of the ratio between the mean absorbance of treated cells and the mean absorbance of untreated cells. Three independent experiments were performed, and the IC50 values (i.e., concentration half inhibiting cell proliferation) were graphically determined using GraphPad Prism 4 software.

4.2.3. PD-L1, VEGFR-2, CD-47 and c-Myc relative quantification by flow cytometry

To study the effect of the compounds on every biological target in cancer cell lines compounds were used at 100 μM. For the assay, 10^5 cells per well were incubated for 48 h with the corresponding dose of the tested compound in a total volume of 500 μL of their growth media. To detect membrane PD-L1, VEGFR-2 and CD-47 after cell treatments, they were collected, fixed with 4 % in PBS paraformaldehyde and stained with FITC Mouse monoclonal Anti-Human VEGFR-2 (ab184903), FITC Mouse monoclonal Anti-CD-47 (ab134484) and Alexa Fluor® 647 Rabbit monoclonal Anti-PD-L1 (ab215251). In order to detect c-Myc and total proteins cells were treated with 0,5% in PBS TritonTM X-100 after fixing them, and then it was added the antibody FITC Rabbit monoclonal Anti-c-Myc (ab223913).

4.2.4. Cell viability evaluation in co-cultures

To study the effect of the compounds on cell viability in co-culture with THP-1 cells, 10^5 HT-29 cells line per well were seeded and incubated for 24 h. Then, medium was changed by a cell culture medium supplemented with IFN-γ (10 ng/ml; human, Invitrogen®) containing 5

$\times 10^5$ of THP-1 cells per well and the corresponding compound at 100 μM. For the positive control DMSO was added. After 48 h of incubation, supernatants were collected to determine THP-1 living cells. Besides, stain cancer cells were collected with trypsin. Both types of suspension cells were fixed with 4 % in PBS paraformaldehyde and counted by flow cytometry.

4.2.5. IL-6 secreted relative quantification by ELISA assay

To study the effect of the compounds on secreted IL-6, 10^5 cells per well were incubated for 48 h with the corresponding dose of the tested compound in a total volume of 500 μL of their growth media. These media were collected and used as a sample in the Invitrogen® Human IL-6 ELISA Kit (Cat: KHC0061).

4.2.6. Antiangiogenic effect

Wells of an IBIDI μ-slide angiogenesis (IBIDI, Martinsried, Germany) were coated with 12 μL of Matrigel® (10 mg/mL, BD Biosciences) at 4 °C. After gelatinization at 37 °C for 30 min, HMEC-1 cells were seeded at 2×10^4 cells/well in 25 μL of culture medium on top of the Matrigel and were incubated 30 min at 37 °C while are attached. Then, compounds were added dissolved in 25 μL of culture medium and after 24 h of incubation at 37 °C, tube destruction was evaluated.

4.2.7. Effect over the antivasulogenic mimicry

80 μL of culture medium were added to each well of Corning® Matrigel® Matrix Cellware plate and were incubated at 37 °C for 24 h. After removing the culture medium, 5×10^4 cells/well were seeded in 80 μL of culture medium and it was incubated at 37 °C for 24 h for the formation of the microvessels. Then, compounds were added dissolved in 20 μL of culture medium and after 24 h of incubation at 37 °C, inhibitory effect on the vasculogenic mimicry was evaluated.

4.2.8. Statistical analysis

Statistical significance was evaluated using one-way ANOVA. Data were expressed as means ± SD for triplicates. The level of statistical significance differences was set as P values of $p < 0.05$.

Author Contributions

All authors have read and agreed to the publication. Eva Falomir: conceptualization, data curation, funding acquisition, formal analysis, investigation, methodology, project administration, resources, software, supervision, validation, visualization, writing-original draft, writing-review & editing. Miguel Carda: conceptualization, data curation, funding acquisition, methodology, project administration, resources, supervision, writing-original draft, writing-review & editing. Alberto Pla-López: data curation, formal analysis, investigation, resources, software, validation, visualization, writing-original draft, writing-review & editing. Paula Martínez-Colomina, Laura Cañada-García, Laura Fuertes-Monge, José Carlos Orellana-Palacios, Alejandro Valderrama-Martínez, Marikena Pérez-Sosa: synthesis and IC_{50} determination.

Funding

This work was supported by the Grant PID2021-126277OB-100 funded by MCIN/AEI/ https://doi.org/10.13039/501100011033 and by "ERDF A way of making Europe" and by Universitat Jaume I (project UJI-B2021-46). A.P-L. appreciates the FPI contract from Generalitat Valenciana (ACIF/2020/341). P.M–C. thanks Universitat Jaume I for the Juan Murga Clausell in memoriam fellowship (UJI-2022).

Declaration of Competing Interest

The authors declare that they have no known competing financial interests or personal relationships that could have appeared to influence the work reported in this paper.

Data availability

No data was used for the research described in the article.

Acknowledgments

Authors are grateful to SCIC of the Universitat Jaume I for providing NMR, mass spectrometry and flow cytometry facilities.

Appendix A. Supplementary data

Supplementary Materials: Analytical spectroscopic data of all new synthetic compounds are provided in the Supplementary Information. Supplementary data to this article can be found online at https://doi.org/10.1016/j.bmc.2023.117490.

References

1 Giraldo NA, Sanchez-Salas R, Peske JD, et al. The clinical role of the TME in solid cancer. *Br J Cancer*. 2019;120:45–53. https://doi.org/10.1038/s41416-018-0327-z.
2 Xiao Y, Yu D. Tumor microenvironment as a therapeutic target in cancer. *Pharmacol Ther*. 2021;221, 107753. https://doi.org/10.1016/j.pharmthera.2020.107753.
3 Baghban R, Roshangar L, Jahanban-Esfahlan R, et al. Tumor microenvironment complexity and therapeutic implications at a glance. *Cell Commun Signal*. 2020;18:1–19. https://doi.org/10.1186/s12964-020-0530-4.
4 Wang M, Zhao J, Zhang L, et al. Role of tumor microenvironment in tumorigenesis. *J Cancer*. 2017;8:761–773. https://doi.org/10.7150/jca.17648.
5 Yi M, Niu M, Xu L, Luo S, Wu K. Regulation of PD-L1 expression in the tumor microenvironment. *J Hematol Oncol*. 2021;14:1–13. https://doi.org/10.1186/s13045-020-01027-5.
6 Jiang Z, Sun H, Yu J, Tian W, Song Y. Targeting CD47 for cancer immunotherapy. *J Hematol Oncol*. 2021;14:1–18. https://doi.org/10.1186/s13045-021-01197-w.
7 Yu L, Ding Y, Wan T, Deng T, Huang H, Liu J. Significance of CD47 and Its Association With Tumor Immune Microenvironment Heterogeneity in Ovarian Cancer. *Front Immunol*. 2021;12, 768115. https://doi.org/10.3389/fimmu.2021.768115.
8 Meškytė EM, Keskas S, Ciribilli Y. MYC as a multifaceted regulator of tumor microenvironment leading to metastasis. *Int J Mol Sci*. 2020;21:7710. https://doi.org/10.3390/ijms21207710.
9 Zhao Y, Guo S, Deng J, et al. VEGF/VEGFR-targeted therapy and immunotherapy in non-small cell lung cancer: targeting the tumor microenvironment. *Int J Biol Sci*. 2022;18:3845. https://doi.org/10.7150/ijbs.70958.
10 Yang J, Yan J, Liu B. Targeting VEGF/VEGFR to modulate antitumor immunity. *Front Immunol*. 2018;9:978. https://doi.org/10.3389/fimmu.2018.00978.
11 Fisher DT, Appenheimer MM, Evans SS. The two faces of IL-6 in the tumor microenvironment. *Semin Immunol*. 2014;26:38–47. https://doi.org/10.1016/j.smim.2014.01.008.
12 Chonov DC, Ignatova MMK, Ananiev JR, Gulubova MV. IL-6 Activities in the tumour microenvironment. Part 1. *Open Access Maced J Med Sci*. 2019;7:2391. https://doi.org/10.3889/oamjms.2019.589.
13 Hirano T. IL-6 in inflammation, autoimmunity and cancer. *Int Immunol*. 2021;33:127–148. https://doi.org/10.1093/intimm/dxaa078.
14 Liu Q, Yu S, Li A, Xu H, Han X, Wu K. Targeting interlukin-6 to relieve immunosuppression in tumor microenvironment. *Tumor Biol*. 2017;39:1–11. https://doi.org/10.1177/1010428317712445.
15 Martín-Beltrán C, Gil-Edo R, Hernández-Ribelles G, et al. Aryl Urea Based Scaffolds for Multitarget Drug Discovery in Anticancer Immunotherapies. *Pharm*. 2021;14:337. https://doi.org/10.3390/ph14040337.
16 Conesa-Milián L, Falomir E, Murga J, Carda M, Marco JA. Novel multitarget inhibitors with antiangiogenic and immunomodulator properties. *Eur J Med Chem*. 2019;148:87–98. https://doi.org/10.1016/j.ejmech.2019.03.012.
17 Pla-López A, Castillo R, Cejudo-Marín R, et al. Synthesis and biological evaluation of small molecules as potential anticancer multitarget agents. *Int J Mol Sci*. 2022;23:7049. https://doi.org/10.3390/ijms23137049.
18 Gil-Edo R, Royo S, Carda M, Falomir E. Unveiling the potential of BenzylethyleneAryl–urea scaffolds for the design of new Onco immunomodulating agents. *Pharm*. 2023;16:808. https://doi.org/10.3390/ph16060808.
19 Gil-Edo R, Hernández-Ribelles G, Royo S, et al. Exploring BenzylethoxyAryl urea scaffolds for multitarget immunomodulation therapies. *Int J Mol Sci*. 2023;24:8582. https://doi.org/10.3390/ijms24108582.
20 Gil-Edo R, Espejo S, Falomir E, Carda M. Synthesis and biological evaluation of potential oncoimmunomodulator agents. *Int J Mol Sci*. 2023;24:2614. https://doi.org/10.3390/ijms24032614.
21 Gadaleta-Caldarola G, Infusino S, Divella R, Ferraro E, Mazzocca A, De Rose F. Sorafenib: 10 years after the first pivotal trial. *Future Oncol*. 2015;11:1863–1880. https://doi.org/10.2217/fon.15.85.
22 Carrato-Mena A, Grande-Pulido E, Guillén-Ponce C. Understanding the molecular-based mechanism of action of the tyrosine kinase inhibitor: sunitinib. *Anticancer Drugs*. 2010;21:3–11. https://doi.org/10.1097/01.cad.0000361534.44052.c5.
23 Zak KM, Grudnik P, Guzik K, et al. Structural basis for small molecule targeting of the programmed death ligand 1 (PD-L1). *Oncotarget*. 2016;7:30323–30335. https://doi.org/10.18632/oncotarget.8730.
24 Patowary P, Deka B, Bharali D. Tetrazole Moiety as a pharmacophore in medicinal chemistry: a review. *Malar Contr Elimin*. 2021;10:5–16. https://doi.org/10.37421/2470-6965.2021.10.167.

25 Kabi AK, Sravani S, Gujjarappa S. et al. An Overview on Biological Evaluation of Tetrazole Derivatives. Nanostructured Biomaterials: Basic Structures and Applications, Springer Nature Singapore 2022, 307-349. ISBN: 978-981-16-8401-2.
26 Fernández-Cortés M, Delgado-Bellido D, Oliver F. Vasculogenic mimicry: Become an endothelial cell "But not so much" Front Oncol., 2019, 22, 9-19. DOI: 3389/fonc.2019.00803.
27 Qiao L, Liang N, Zhang J, et al. Advanced research on vasculogenic mimicry in cancer. *J Cell Mol Med*. 2015;19:315–326. https://doi.org/10.1111/jcmm.12496.
28 Folberg R, Hendrix MJ, Manioti AJ. Vasculogenic mimicry and tumor angiogenesis. *Am J Pathol*. 2000;156:361–381. https://doi.org/10.1016/S0002-9440(10)64739-6.
29 Nepali K, Lee HY, Liou JP. Nitro-Group-Containing Drugs. *J Med Chem*. 2019;62:2851–2893. https://doi.org/10.1021/acs.jmedchem.8b00147.
30 Noriega S, Cardoso-Ortiz J, López-Luna A, Cuevas-Flores MDR, Flores De La Torre JA. The diverse biological activity of recently synthesized nitro compounds. *Pharmaceuticals*. 2022;15:717. https://doi.org/10.3390/ph15060717.
31 Rice AM, Long Y, King SB. Nitroaromatic antibiotics as nitrogen oxide sources. *Biomolecules*. 2021;11:267. https://doi.org/10.3390/biom11020267.